Spectrum and screening cloud in the central spin model

Michael Bortz,[1,*] Sebastian Eggert,[1] and Joachim Stolze[2]
[1]*Fachbereich Physik und Research Center OPTIMAS, Technische Universität Kaiserslautern, Erwin-Schrödinger-Strasse, D-67663 Kaiserslautern, Germany*
[2]*Institut für Physik, Technische Universität Dortmund, D-44221 Dortmund, Germany*

(Received 10 September 2009; revised manuscript received 25 November 2009; published 11 January 2010)

We consider an electronic spin in a quantum dot, coupled to the surrounding nuclear spins via inhomogeneous antiferromagnetic hyperfine interactions and subject to a uniform field, which is described by Gaudin's central spin model. We study spectral properties, the two-point correlation functions, and the magnetization profile in the ground state and in low-lying excited states, which characterizes the structure of the cloud of nuclear spins screening the electron spin. A close connection to the pair-occupation probability in the BCS model is established. Using the exact Bethe-Ansatz solution of that model and arguments of integrability, we can distinguish between contributions from purely classical physics and from quantum fluctuations.

DOI: 10.1103/PhysRevB.81.035315 PACS number(s): 73.21.La, 02.30.Ik

I. INTRODUCTION

Over the last decade, experimental realizations of strongly correlated quantum systems have led to the possibility of studying nonequilibrium quantum processes on a microscopic level. From a theoretical point of view, the description of such processes is challenging because it requires a thorough study of the spectrum and correlation functions.

In this work, we consider a model which describes the hyperfine interaction of an electron spin (the central spin) in a quantum dot with a bath of nuclear spins in the dot. The resulting Heisenberg exchange interaction is dominant for short-time scales up to 1 ms before other mechanisms such as spin-orbit coupling or dipole-dipole interactions between the bath spins.[1–4] This is an ideal system to generally understand the decoherence of a qubit which is realized by the electron spin[5] and in this context the loss of quantum information. Many important contributions on this central issue have been made by a number of authors using different methods[4,6–19] as also outlined in the reviews, Refs. 20 and 21. All those works rely on often very sophisticated approximation schemes to study the time evolution of the central spin directly. In this work, our goal is to use the *exact* solution of the model to study its spectrum and static correlation functions in the ground state and excited states also in comparison with a simple classical approximation. In the future, this knowledge can be used to obtain exact information about nonequilibrium dynamics such as the decoherence process.

The central spin model (or Gaudin model[22,23]) we consider here describes the isotropic Heisenberg coupling of the central electron spin $\boldsymbol{S}_0$ with inhomogeneous exchange couplings A_j to a bath of N_b nuclear spins $\boldsymbol{S}_{j=1,\ldots,N_b}$. The nuclei are assumed to be spin-1/2 particles and their coupling g_{n} to the external magnetic field h is assumed to be much weaker than that of the electron, g_{e}

$$H=\sum_{j=1}^{N_b} A_j \boldsymbol{S}_0\cdot\boldsymbol{S}_j - hg_{\mathrm{e}}S_0^z - hg_{\mathrm{n}}\sum_{j=1}^{N_b} S_j^z. \tag{1}$$

The couplings A_j are proportional to the square of the electronic wave function at the positions of the nuclei. For a realistic distribution of the A_j, we can think of the index j as measuring the distance from the center of the dot. The methods we use in this work, especially the classical approach and the integrability, do not depend on the choice of couplings A_j but for definiteness we assume a harmonic trapping potential for the electron. This results in a Gaussian decay of the couplings[10]

$$A_j=\alpha\exp[-(jB/N_b^{1/D})^2], \tag{2}$$

where the normalization $\alpha=x_1N_b/\sum_{j=1}^{N_b}\exp[-(jB/N_b^{1/D})^2]$ is chosen such that the mean value (or first moment) x_1 of the A_j is fixed and the dimension is taken $D=1$. Here, the parameter B controls the degree of inhomogeneity. We will choose $B=2$ and $x_1=2$ as generic values for inhomogeneous couplings and $B=2/5$ and $x_1=2$ as parameters for nearly homogeneous couplings in numerical diagonalizations in later sections.

We calculate the spectrum, the magnetization profile $\langle S_j^z\rangle$ of the nuclear bath spins and the two-point functions $\langle \boldsymbol{S}_0\cdot\boldsymbol{S}_j\rangle$ of the model in Eq. (1). It is possible to distinguish two types of contributions in these quantities: on the one hand, terms appear that can be obtained from a purely classical approach. Additionally, we identify terms stemming from quantum fluctuations. Most importantly, classical and quantum terms can be of the same order in the two-point function.

This paper is organized as follows. In Sec. II, we show how to obtain one- and two-point functions from the exact Bethe-Ansatz solution for the eigenvalues and eigenstates of the Hamiltonian (1). The central-spin and BCS-pairing models are linked by their integrability which provides a way to calculate the magnetization profile $\langle S_j^z\rangle$. Two-point functions are given by derivatives of the energy with respect to the Heisenberg coupling constants.

In Sec. III, we evaluate one- and two-point correlation functions based on a classical picture which, for finite magnetic field, assumes spontaneous symmetry breaking in the model (1), similar to the superconducting phase transition in the closely related BCS model. The local magnetization obtained by completely diagonalizing the quantum-mechanical model with 16 spins agrees very well with the classical results. However, for the two-point function, the agreement is less good, which indicates that quantum fluctuations are of the same order as the classical terms.

We are thus led to study the exact solution in Sec. IV, especially in order to obtain quantum-mechanical contributions to correlation functions. This is done for zero and finite magnetic fields. The connection with the classical approach is also established. The paper ends with an outlook.

II. EXACT SOLUTION, LINK TO THE BCS MODEL AND CORRELATION FUNCTIONS

A. Exact solution

With a special focus on the magnetic field terms, we rewrite Eq. (1) as

$$H=\sum_{j=1}^{N_b} A_j \boldsymbol{S}_0\cdot\boldsymbol{S}_j - h_0 S_0^z - h_t S_{\mathrm{tot}}^z \tag{3}$$

with $h_0=h(g_e-g_n)$, $h_t=hg_n$, and the total polarization $S_{\mathrm{tot}}^z=\Sigma_{j=0}^{N_b}S_j^z=\frac{N}{2}-M$, where $N=N_b+1$ is the total number of spins and M is the number of flipped spins compared to the ferromagnetic all-up state. Note that S_{tot}^z commutes with the Hamiltonian

$$[H,S_{\mathrm{tot}}^z]=0 \tag{4}$$

and thus $S_{\mathrm{tot}}^z=N/2-M$ is a constant of motion. This means that the last term in Eq. (3) provides an additive constant which we will drop in the following unless otherwise stated.

The model in Eq. (3) has been solved by Gaudin[22,23] using a coordinate-type Bethe-Ansatz; an algebraic solution has been given by Sklyanin[24] and is also described in Ref. 25. The exact solution has been used in Ref. 26 to calculate nonequilibrium dynamics in a fully polarized bath. Using the notation from Ref. 26, the eigenvalues Λ in a sector of given M read

$$\Lambda=-\frac{1}{2}\sum_{k=0}^{M_b}\omega_k+\frac{N_b x_1}{4}-\frac{h_0}{2}, \tag{5}$$

where x_1 is the mean value of the A_j and $M_b:=M-1$. The set of the ω_k, $k=0,\ldots,M_b$, is determined by the Bethe-Ansatz equations (BAE)

$$1+\sum_{j=1}^{N_b}\frac{A_j}{A_j-\omega_k}-2\sum_{k'\neq k}^{M_b}\frac{\omega_{k'}}{\omega_{k'}-\omega_k}+\frac{2h_0}{\omega_k}=0. \tag{6}$$

Gaudin[27] showed that there are $C_M^N=N!/[M!(N-M)!]$ sets of solutions $\{\omega_0,\ldots,\omega_{M_b}\}$ to these equations in each sector of given M, one for each eigenvalue Λ. The corresponding energy eigenstates with a fixed number M of flipped spins are given by

$$|M\rangle=\frac{1}{n_M}\prod_{k=0}^{M_b}\left[-S_0^-+\sum_{j=1}^{N_b}\frac{A_j}{\omega_k-A_j}S_j^-\right]|0\rangle, \tag{7}$$

where $|0\rangle$ is the fully polarized state $|\Uparrow;\uparrow,\ldots,\uparrow\rangle$, and the arrows $\Uparrow,\Downarrow$ for the central spin and $\uparrow,\downarrow$ for the bath spins are used. The normalization factor n_M was conjectured by Gaudin[23,27] and proved by Sklyanin[28] for $h_0=0$

$$n_M^2=(-1)^M\det\mathcal{M},$$

$$\mathcal{M}_{kk}=-1-\sum_{j=1}^{N_b}\frac{A_j^2}{(\omega_k-A_j)^2}+\sum_{k'\neq k}\frac{2\omega_{k'}^2}{(\omega_k-\omega_{k'})^2},$$

$$\mathcal{M}_{kk'}=-\frac{2\omega_{k'}^2}{(\omega_k-\omega_{k'})^2},\quad k\neq k'.$$

In Ref. 26 evidence was given that this holds for finite h_0 as well.

Let us now come back to the eigenvalues in Eq. (5). Due to the Hellmann-Feynman theorem,[29–32] two-point correlators between the central spin and a bath spin in an eigenstate are obtained as the derivatives of the energy eigenvalues

$$\langle\boldsymbol{S}_0\cdot\boldsymbol{S}_j\rangle=\partial_{A_j}\Lambda=-\frac{1}{2}\sum_{k=0}^{M_b}\partial_{A_j}\omega_k+\frac{1}{4}, \tag{8}$$

using Eq. (5) in the second step and the expectation value of the central spin polarization is given by

$$\langle S_0^z\rangle=-\partial_{h_0}\Lambda. \tag{9}$$

By solving the BAE Eq. (6) as a function of the couplings A_j and the field h_0 it is therefore possible to obtain the expectation values directly.

In order to also calculate the magnetization profile $\langle S_j^z\rangle$, $j=1,\ldots,N_b$ we have to use some additional features of the integrable structure of the model in Eq. (3), as will be described in the remainder of this section. Let us rewrite Eq. (3) in the original notation used by Gaudin[23]

$$H_\ell=-\sum_{j=0,j\neq\ell}^{N_b}\frac{\boldsymbol{S}_\ell\cdot\boldsymbol{S}_j}{\varepsilon_\ell-\varepsilon_j}-h_0S_\ell^z \tag{10}$$

such that we recover Eq. (3) with $h_t=0$ for

$$A_j=1/\varepsilon_j \tag{11}$$

and $\ell=0$ and $\varepsilon_0=0$ in Eq. (10). As pointed out by Gaudin[23]

$$[H_\ell,H_{\ell'}]=0, \tag{12}$$

which means that an integrable Hamiltonian can be constructed as a linear combination of N mutually commuting conserved quantities

$$\tilde{H}:=\sum_{\ell=0}^{N_b}\varepsilon_\ell H_\ell=-h_0\sum_{\ell=0}^{N_b}\varepsilon_\ell S_\ell^z-\frac{1}{2}(\boldsymbol{S}_{\mathrm{tot}})^2+\frac{1}{2}\sum_{\ell=0}^{N_b}\boldsymbol{S}_\ell^2 \tag{13}$$

with $\boldsymbol{S}_{\mathrm{tot}}=\Sigma_{\ell=0}^{N_b}\boldsymbol{S}_\ell$.

The model in Eq. (13), has the same eigenstates as the original model in Eq. (3), even though these are not necessarily in the same energetic order. For the local expectation values, one can apply the Hellmann-Feynman theorem[29–32] to the eigenvalues $\tilde{\Lambda}$ of $\tilde{H}$

$$\langle S_j^z\rangle = -\frac{1}{h_0}\partial_{\varepsilon_j}\tilde{\Lambda} = -\frac{1}{h_0}\partial_{A_j^{-1}}\tilde{\Lambda}. \tag{14}$$

In order to calculate $\tilde{\Lambda}$, we use Gaudin's result[22] for the eigenvalues $\Lambda^{(\ell)}$ of H_ℓ in Eq. (10)

$$\Lambda^{(\ell)} = \frac{1}{2}\sum_{k=0}^{M_b}\frac{1}{\varepsilon_\ell - E_k} - \frac{1}{4}\sum_{j=0,j\neq\ell}^{N_b}\frac{1}{\varepsilon_\ell-\varepsilon_j} - \frac{h_0}{2} \tag{15}$$

with

$$E_k = 1/\omega_k \tag{16}$$

such that

$$\tilde{\Lambda} = \sum_{\ell=0}^{N_b}\varepsilon_\ell\Lambda^{(\ell)} = \frac{1}{2}\sum_{\ell,k}\frac{\varepsilon_\ell}{\varepsilon_\ell - E_k} - \frac{N_b(N_b+1)}{8} - \frac{h_0}{2}\sum_{\ell=0}^{N_b}\varepsilon_\ell. \tag{17}$$

By rewriting the BAE Eq. (6) in terms of the ε_j, E_k and defining $g \coloneqq 1/h_0$, we arrive at

$$\sum_{j=0}^{N_b}\frac{1}{E_k-\varepsilon_j} - 2\sum_{k'\neq k}\frac{1}{E_k - E_{k'}} + \frac{2}{g} = 0. \tag{18}$$

Observing that $\varepsilon_j/(E_k-\varepsilon_j)=E_k/(E_k-\varepsilon_j)-1$ and $E_k/(E_k-E_{k'})+E_{k'}/(E_{k'}-E_k)=1$ we can eliminate the first term in Eq. (17) by multiplying Eq. (18) with E_k and then performing the sum over k. Hence Eq. (17) becomes

$$\tilde{\Lambda} = h_0\sum_{k=0}^{M_b}E_k - \frac{h_0}{2}\sum_{\ell=1}^{N_b}\varepsilon_\ell - \frac{M_b(M_b+1)}{4} - \frac{N_b(N_b+1)}{8} + \frac{(N_b+1)(M_b+1)}{2}, \tag{19}$$

which yields, together with Eq. (14)

$$\langle S_j^z\rangle = \frac{1}{2} - \partial_{\varepsilon_j}\sum_{k=0}^{M_b}E_k = \frac{1}{2} - \partial_{1/A_j}\sum_{k=0}^{M_b}\frac{1}{\omega_k}. \tag{20}$$

In summary it is therefore possible to express the two-point function, Eq. (8), and the local magnetization Eq. (20) in terms of the BA numbers of the exact solution, which is the main finding of this section. These quantities will be analyzed in detail in Secs. III and IV.

B. Link to the BCS-pairing model

It is possible to relate spin with fermionic operators, using Anderson spin-1/2 pseudospin operators[25,33]

$$S_j^z = \frac{1}{2}(1 - c_{j\uparrow}^\dagger c_{j\uparrow} - c_{j\downarrow}^\dagger c_{j\downarrow}), \tag{21}$$

$$S_j^- = c_{j\uparrow}^\dagger c_{j\downarrow}^\dagger, \quad S_j^+ = c_{j\downarrow}c_{j\uparrow}, \tag{22}$$

which preserve the SU(2) commutators $[S_i^+,S_j^-]=2\delta_{ij}S_j^z$ and $[S_i^z,S_j^\pm]=\pm\delta_{ij}S_j^\pm$.[25]

A BCS-like Hamiltonian can be defined by rescaling the integrable model $\tilde{H}$ from Eq. (13)

$$H_{\rm BCS} \coloneqq \frac{1}{h_0}\tilde{H} + \frac{1}{2}\sum_{\ell=0}^{N_b}\varepsilon_\ell + \frac{S_{\rm tot}^z(S_{\rm tot}^z+1)}{2h_0} - \frac{3(N_b+1)}{8h_0}, \tag{23}$$

where $S_{\rm tot}^z = N_b/2 - M_b - 1/2$ is the conserved quantum number from Eq. (3). In terms of spin operators $H_{\rm BCS}$ therefore reads

$$H_{\rm BCS} = -\sum_{j=0}^{N_b}A_j^{-1}\left(S_j^z - \frac{1}{2}\right) - \frac{1}{2h_0}(\mathbf{S}_{\rm tot})^2 + \frac{1}{2h_0}S_{\rm tot}^z(S_{\rm tot}^z+1). \tag{24}$$

Replacing the spin operators using Eqs. (21) and (22), one arrives at the fermionic representation

$$H_{\rm BCS} = \frac{1}{2}\sum_{\substack{\ell=0\\ \sigma=\uparrow,\downarrow}}^{N_b}\varepsilon_\ell c_{\ell\sigma}^\dagger c_{\ell\sigma} - \frac{g}{2}\sum_{\ell,j=0}^{N_b}c_{\ell\downarrow}^\dagger c_{\ell\uparrow}^\dagger c_{j\uparrow}c_{j\downarrow} \tag{25}$$

with the doubly degenerate single-particle levels ε_ℓ and the pairing amplitude $g=1/h_0$.[34]

Hamiltonian (25) describes M pairs of fermionic particles interacting via an attractive pairing potential thus affecting the N doubly degenerate energy levels ε_j. In a series of papers, Richardson[35–40] used it to describe pairing in nuclei. In the more recent past, the exact solution of this model has been rediscovered to study ultrasmall metallic grains in their superconducting phase.[41] In the thermodynamic limit, the solution of the model in Eq. (23), yields the mean-field BCS solution;[42] we will come back to this point in Sec. III.

From Eqs. (14) and (23) it follows that the occupation probability $\langle n_j\rangle \coloneqq \langle c_{j\uparrow}^\dagger c_{j\uparrow} + c_{j\downarrow}^\dagger c_{j\downarrow}\rangle/2$ of the single-particle level ε_j reads[40,43]

$$\langle n_j\rangle = \partial_{\varepsilon_j}\langle H_{\rm BCS}\rangle = \frac{1}{2} - \langle S_j^z\rangle, \tag{26}$$

which is consistent with Eq. (21). Thus the single-particle occupation numbers in the pairing model are directly related to the local polarization of nuclear spins in the central spin model.

We will compute two-point correlation functions and the magnetization profile for different parameter regimes in the following sections. For illustrative purposes, let us first check the extreme limits $h_0\to 0,\infty$ in Eq. (26) for the ground state in the sector $S_{\rm tot}^z=0$ (this implies that we take N to be even here). In the BCS model, this corresponds to the case of half filling, where the number of electrons $2M$ equals the number of free-particle levels N. For $h_0\to 0$, the model in Eq. (3), is SU(2) invariant so $\langle S_j^z\rangle|_{h_0=0}=0$. Since $g=1/h_0$, the pairing potential is infinitely strong in this limit, such that all levels are occupied and only ideal Cooper pairs exist, where each level is occupied by half a pair.

In the opposite limit, $h_0\to\infty$, the central spin is frozen along the z direction. The directions of the bath spins are simply given by the competition of the antiferromagnetic exchange in Eq. (3) with the magnetic field h_t. Therefore, all outer bath spins with coupling $A_j < 2h_t$ are aligned with the field and the central spin while the inner ones point in the

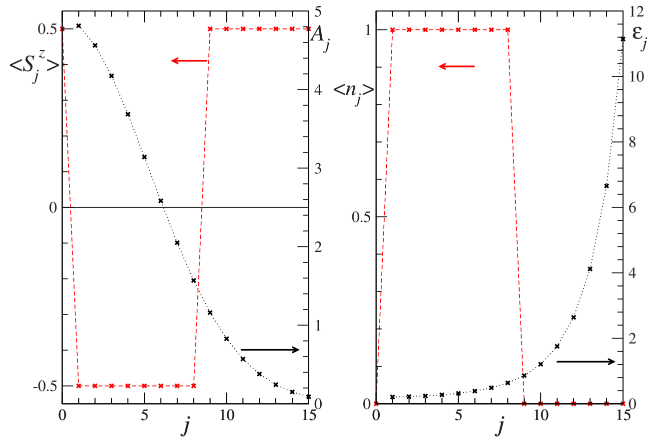

FIG. 1. (Color online) Left panel: magnetization profile in a quantum dot with $N_b=15$, infinite central magnetic field, $h_0\to\infty$, and total field $A_8>2h_t>A_9$. The black crosses denote the coupling constants chosen according to Eq. (2) with $x_1=2$, $B=2$. Right panel: corresponding electronic occupation probability according to Eq. (26) for free Fermions with (black crosses) the single-particle levels ε_j, $j=1,\ldots,N_b$, according to Eqs. (2) and (11). The system is in a two-particle excited state, where the pair occupying the lowest energy level $\varepsilon_0=0$ is shifted to the energetically lowest state above the Fermi level.

opposite direction. The resulting magnetization profile is sketched schematically in the left panel of Fig. 1, where we chose $A_{(N_b+1)/2}>2h_t>A_{(N_b+1)/2+1}$, such that $S^z_{\rm tot}=0$ for illustrative purposes.

For the BCS model in Eq. (25), this means that the highest states where ε_j is largest (i.e., $A_j=1/\varepsilon_j$ is smallest) are unoccupied. This is the filled Fermi sea for the noninteracting Fermi gas. The level $\varepsilon_0=0$ is special in the sense that it is unoccupied in the ground state of the central spin model, which is an excited state in terms of the BCS Hamiltonian. From this we conclude that the ground state of the central spin model for $S^z_{\rm tot}=0$ corresponds to an excited state of the BCS model where the energetically lowest pair is shifted to the top of the filled Fermi sea. This is illustrated in the right panel of Fig. 1 and will be further discussed in Sec. IV C.

III. THE SCREENING CLOUD FROM A CLASSICAL POINT OF VIEW

In this section, we develop a classical picture for the energy and the magnetization profile of the model in Eq. (3), for finite magnetic fields, which turns out to be closely related to the mean-field BCS solution[42] of the pairing Hamiltonian (25).

It is reasonable to expect that for large coordination number $N_b\gg 1$, a classical approach to the Hamiltonian (3) yields valuable insights into the physics of the model.[44] The classical approach consists of replacing quantum-mechanical spin operators $\boldsymbol{S}_j$ by classical vectors $\langle \boldsymbol{m}_j\rangle$. Especially, for states with the same quantum number $S^z_{\rm tot}$, an expectation value $\langle S^x_j\rangle\neq 0$ implies that in this limit, the Hamiltonian symmetry Eq. (4) is spontaneously broken. This mechanism is analogous to the superconducting phase transition in which particle-number conservation is broken, $\langle c^\dagger_{j\uparrow}c^\dagger_{j'\downarrow}\rangle\neq 0$.

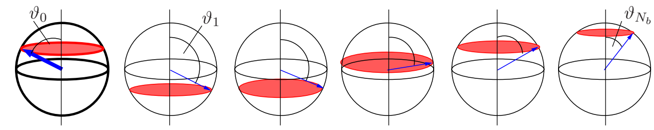

FIG. 2. (Color online) Schematic orientation of the classical spins according to Eqs. (36) and (37). The fat leftmost spin is the center of the dot. The central field leads to a canting of the central spin, which, due to the antiferromagnetic exchange, leads to an opposite canting of the neighboring spins. Since an overall magnetic field is included which fixes the total magnetization, a nontrivial magnetization profile results.

A. Magnetization pattern in the central spin model

Let us begin by parameterizing each spin in polar coordinates, $\boldsymbol{m}_j=\frac{1}{2}(\cos\varphi_j\sin\vartheta_j,\sin\varphi_j\sin\vartheta_j,\cos\vartheta_j)$ such that $|\boldsymbol{m}_j|^2=\frac{1}{4}$ for $j=0,\ldots,N_b$. Our aim is to derive the ground-state configuration described by the angles φ_j,ϑ_j for a given total magnetization $S^z_{\rm tot}$ and fixed central field h_0.

The classical energy as a function of the azimuthal angles φ_j is always minimized by choosing $\varphi_0-\varphi_j=\pi$, corresponding to antiferromagnetic alignment in the xy plane. The resulting classical model for the polar angles analogous to Eq. (3) is then given by

$$H_{\rm cl}=\frac{1}{4}\sum_{j=1}^{N_b}A_j\cos(\vartheta_0+\vartheta_j)-\frac{h_0}{2}\cos\vartheta_0-\frac{h_t}{2}\sum_{j=0}^{N_b}\cos\vartheta_j \tag{27}$$

and the total magnetization can be determined from

$$2S^z_{\rm tot}=\sum_{j=0}^{N_b}\cos\vartheta_j. \tag{28}$$

The first antiferromagnetic term in Eq. (27) is minimized by large polar angles $\vartheta_0+\vartheta_j=\pi$, i.e., spins lying in the xy plane while the field tends to keep the polar angles small, analogous to the situation in a two-dimensional Heisenberg antiferromagnet with a central impurity.[45] For finite fields the central spin typically acquires a relatively small but finite polar angle while the bath spins cant into the opposite direction out of the plane with polar angles that are closer to $\pi/2$. Depending on the overall magnetic field this results in a characteristic magnetization profile: those bath spins which are coupled strongly are aligned antiferrogmagnetically to the central spin (i.e., against the field) while the more loosely bound bath spins at the edge of the dot are aligned ferromagnetically. Depending on the parameters the total magnetization $S^z_{\rm tot}$ is often quite small or even negative. A typical resulting magnetization profile is sketched in Fig. 2.

The optimum values of the angles are most easily found by requiring that the total value of the torque $|\boldsymbol{\tau}_0|$ experienced by the central spin from the central field and the bath spins has to vanish

$$|\boldsymbol{\tau}_0|=\partial_{\vartheta_0}H_{\rm cl}=0, \tag{29}$$

$$\Rightarrow h_0 \sin \vartheta_0 = \frac{1}{2}\sum_{j=1}^{N_b} A_j \sin(\vartheta_j + \vartheta_0) - h_t \sin \vartheta_0. \quad (30)$$

Equally well, the torque on each individual bath spin is zero in equilibrium

$$|\boldsymbol{\tau}_j| = \partial_{\vartheta_j} H_{cl} = 0 \quad (31)$$

$$\Rightarrow h_t \sin \vartheta_j = \frac{A_j}{2}\sin(\vartheta_j + \vartheta_0) \quad (j \neq 0). \quad (32)$$

Obviously, Eqs. (30) and (32) are trivially fulfilled when $\vartheta_{j=0,\ldots,N_b}$ are integer multiples of π. We exclude these solutions here because generally they do not correspond to minima of the energy as can be seen from the Hesse matrix of second derivatives of H_{cl}.

We now insert Eqs. (30) and (32) into Eq. (27) and obtain

$$H_{cl} = -\frac{1}{4}\sum_{j=1}^{N_b} A_j \frac{\sin \vartheta_j}{\sin \vartheta_0} - \frac{1}{4}\sum_{j=1}^{N_b} A_j \cot \vartheta_j \sin(\vartheta_0 + \vartheta_j). \quad (33)$$

From Eqs. (30) and (32) it follows that if the fields $h_{0,t}$ are given, then we can solve for the angles ϑ_j, which are given by

$$\tan \vartheta_j = \frac{\delta A_j}{\nu - A_j}, \quad (34)$$

where

$$\delta = \tan \vartheta_0, \quad \nu = 2h_t/\cos \vartheta_0. \quad (35)$$

The angles in Eq. (34) show the generic behavior described above unless extreme values of the parameters are assumed: the magnetization changes from alignment with the field for the outermost bath spins ($A_j \to 0$) through the xy plane ($A_j \sim \nu$) to near antiferromagnetic alignment for the most strongly coupled spins near the center ($A_j > \nu$).

The components of the magnetization along the field m^z and in the plane $m^\perp$ can be found explicitly by using

$$\tan \vartheta_0 = m_0^\perp / m_0^z = \delta, \quad (36)$$

$$\tan \vartheta_j = m_j^\perp / m_j^z = \frac{\delta A_j}{\nu - A_j} \quad \text{for } j = 1, \ldots, N_b \quad (37)$$

from which it follows that

$$m_0^z = \frac{1}{2\sqrt{1+\delta^2}}, \quad m_0^\perp = \frac{\delta}{2\sqrt{1+\delta^2}}, \quad (38)$$

$$m_j^z = \frac{\nu - A_j}{2\sqrt{(\nu - A_j)^2 + (A_j\delta)^2}}, \quad m_j^\perp = \frac{\delta A_j}{2\sqrt{(\nu - A_j)^2 + (A_j\delta)^2}}. \quad (39)$$

Similar equations were obtained using methods of classical integrability in Ref. 44. In order to determine the parameters δ and ν we obtain from Eqs. (38) and (39) for the total magnetization along the field

$$2S_{tot}^z = \frac{1}{\sqrt{1+\delta^2}} + \sum_{j=1}^{N_b} \frac{\nu - A_j}{\sqrt{(\nu - A_j)^2 + (A_j\delta)^2}} \equiv 2N - M. \quad (40)$$

Equation (30) for the central field now reads

$$h_0 = \sum_{j=1}^{N_b} \frac{\nu A_j}{2\sqrt{(\nu - A_j)^2 + (A_j\delta)^2}} - \frac{\nu}{2\sqrt{1+\delta^2}}. \quad (41)$$

Equations (40) and (41) fix δ and ν uniquely for a given S_{tot}^z and h_0 so that all classical vectors are known, which is the central result of this section.

Finally, one obtains the corresponding expression for the energy from Eq. (33) without the trivial h_t term

$$H_{cl} = -\frac{1}{4}\sum_{j=1}^{N_b} \left[\frac{1+\delta^2}{(\nu - A_j)^2 + (A_j\delta)^2}\right]^{1/2} A_j^2. \quad (42)$$

This parametrization of the ground-state energy in terms of ν, δ and the A_j will be helpful in separating classical from pure quantum contributions in the exact solution later on in Sec. IV C.

It is interesting to note that an alternative derivation of Eq. (41) is obtained by considering the magnetic fields $h_{0,t}$ as canonically conjugate to m_0^z and S_{tot}^z so that $h_0 = \partial_{m_0^z} \sum_{j=1}^{N_b} \boldsymbol{m}_0 \cdot \boldsymbol{m}_j$ and $h_t = \partial_{S_{tot}^z} \sum_{j=1}^{N_b} \boldsymbol{m}_0 \cdot \boldsymbol{m}_j$.

The classical spin-spin correlation function between the electron and nuclear spins can be obtained from Eqs. (38) and (39), namely,

$$\boldsymbol{m}_0 \cdot \boldsymbol{m}_j = -\frac{(1+\delta^2)A_j - \nu}{4\sqrt{1+\delta^2}\sqrt{(\nu - A_j)^2 + (A_j\delta)^2}}. \quad (43)$$

B. Connection with the BCS model

Very similar relations were derived[22,40,42] for the thermodynamic limit of the BCS-pairing model Eq. (25)

$$H_{BCS}^{(cl)} = \frac{\Delta^2}{g} + \sum_{j=1}^{N_b} \varepsilon_j - \mu(N - 2M) - \sum_{j=0}^{N_b} \sqrt{(\varepsilon_j - \mu)^2 + \Delta^2}, \quad (44)$$

$$\frac{2}{g} = \sum_{j=0}^{N_b} \frac{1}{\sqrt{(\varepsilon_j - \mu)^2 + \Delta^2}}, \quad (45)$$

$$N - 2M = \sum_{j=0}^{N_b} \frac{\varepsilon_j - \mu}{\sqrt{(\varepsilon_j - \mu)^2 + \Delta^2}}. \quad (46)$$

Here Δ is the superconducting gap, μ is the chemical potential, and $H_{BCS}^{(cl)}$ is the ground-state energy of Eq. (25) in the thermodynamic limit. Equations (45) and (46) are equivalent to Eqs. (40) and (41), if Eq. (11) and the following relations hold

$$\delta = \Delta/\mu, \quad \nu = 1/\mu, \quad h_0 = 1/g \quad (47)$$

and if furthermore, the sign of the $j=0$ term in Eqs. (45) and (46) is changed. The latter condition reflects the fact that the ground state of the central spin model corresponds to a special single-pair excited state of the BCS model. This point will be discussed quantitatively in Sec. IV.

The mechanism of spontaneous symmetry breaking in the classical/mean-field approach is completely equivalent in both the BCS and central spin models. In order to see this, we use the pseudospin representation in Eqs. (21) and (22), to write the BCS gap in the pair-excited state corresponding to the ground state of the central spin model as

$$\Delta = g\sum_{j=1}^{N_b} m_j^{\perp}. \tag{48}$$

Inserting the last of relations in Eq. (39) and substituting Eq. (11) and the first two equations from Eq. (47), one reobtains the gap equation (45).

An important difference to the BCS solution consists in the order of magnitude of $h_0=1/g$. To obtain a well-defined energy per particle in the thermodynamic limit, $1/g=\mathcal{O}(N)$ scales with the number of particles. In the quantum dot, however, the experimental situation corresponds to $h_0=\mathcal{O}(1)$ thus not scaling with any extensive parameter. It is instructive though to consider the limit of infinite central magnetic field, shown in Fig. 1. Then $\delta\to 0$ and from Eq. (41), $h_0\approx\sum_{j=1}^{N_b}|2(\varepsilon_j-\mu)|^{-1}\gg 1$. Furthermore, Eq. (40) yields $A_{N/2}<\nu<A_{N/2+1}$ so that Eqs. (38) and (39) reproduce the magnetization profile shown in Fig. 1. In this extreme limit, quantum fluctuations are suppressed completely and the classical picture is exact. Accordingly, the classical mean-field approximation is generally better justified for the BCS model. However, for general fields $h_0=\mathcal{O}(1)$, apart from the classical contribution discussed in this section, important quantum fluctuations will occur as well as will be shown in the next section.

C. Analytical results: Small field limit

Equations (40) and (41) can be solved numerically to determine the parameters ν and δ from which the magnetization profile Eq. (39) and the two-point function Eq. (43) are obtained. However, in the physically most relevant limit of small central fields and large particle numbers it is useful to derive approximate analytical expressions for the one- and two-point correlators. Therefore, we will first calculate the parameters δ and ν from Eqs. (40) and (41) to leading order in h_0, before inserting these results into Eqs. (39) and (43) for the correlation functions.

According to Eq. (41), a small central magnetic field corresponds to

$$h_0 = \frac{N_b\nu}{2\delta^{(1)}}, \quad \delta^{(1)} = \frac{N_b\nu}{2h_0}, \tag{49}$$

where the index $\delta^{(1)}$ is the leading term of δ in a small-field expansion of δ. Since we derived Eqs. (40) and (41) for a large number of nuclei, we restrict ourselves to the terms leading in N_b here. Equation (49) is consistent with Eq. (47): both imply that a diverging pairing strength in the BCS-pairing model leads to a diverging superconducting gap.

In the same limit, Eq. (40) leads to

$$2\delta^{(1)}S_{\mathrm{tot}}^z = N - \nu N_b x_{-1}, \tag{50}$$

where we defined the moments x_ℓ

$$N_b x_\ell := \sum_{j=1}^{N_b} A_j^{\ell}. \tag{51}$$

The moments with negative (positive) integers ℓ are determined predominately by the smallest (largest) coupling constants.

We consider here a sample which is not macroscopically polarized, i.e., $S_{\mathrm{tot}}^z=\mathcal{O}(1)$. The case of macroscopic polarization will be dealt with in Sec. IV. Together with Eq. (49), we then obtain for the leading term of ν for small fields, $\nu^{(1)}$

$$\frac{1}{\nu^{(1)}} = x_{-1} + \frac{S_{\mathrm{tot}}^z}{h_0}. \tag{52}$$

Making the same approximations in the expression for the classical ground-state energy, Eq. (42), and inserting Eqs. (49) and (52), we obtain the leading term for small h_0

$$H_{\mathrm{cl}}^{(1)} = -\frac{N_b x_1}{4} - h_0\frac{S_{\mathrm{tot}}^z}{N} - \frac{h_0^2}{2N}x_{-1}. \tag{53}$$

For small central fields, this yields the following expressions for the leading terms in a large-N expansion of classical one- and two-point correlation functions in the ground state:

$$\boldsymbol{m}_0\cdot\boldsymbol{m}_j = -\frac{1}{4} + \frac{1}{2}\frac{h_0^2}{(A_jN)^2}, \tag{54}$$

$$m_0^z = \frac{S_{\mathrm{tot}}^z}{N} + \frac{h_0 x_{-1}^{(0)}}{N}, \tag{55}$$

$$m_j^z = -m_0^z + \frac{h_0}{NA_j}, \tag{56}$$

where $x_{-1}^{(0)}$ is the leading term in an asymptotic expansion of x_{-1} in the inverse particle number, $x_{-1}^{(0)} := \int_0^1 1/A(xN_b)dx$, and $A(xN_b)\equiv A_j$ is treated as a continuous function of x.

D. Quantitative comparison with numerical results

We illustrate the classical results in Fig. 3, where magnetization profiles $m_{j=0,\ldots,N_b}^z$ are shown, after solving Eqs. (40) and (41) numerically for $S_{\mathrm{tot}}^z=0$ and different h_0. The small-field asymptotes from Eqs. (55) and (56) are depicted as well. We now discuss the question to what extent these classical expressions can be identified with the quantum-mechanical expectation values for large particle number and small central field.

In order to do so, we first compare our results with a complete diagonalization study for a system with $N=16$ sites as an additional independent check. The coupling constants in this system were chosen according to Eq. (2) with $x_1=2$, $B=2$. In the next section, we will see that the complete diagonalization study also enables us to classify low-lying excited states according to the distribution of the corresponding BA roots, which is not possible *a priori*.

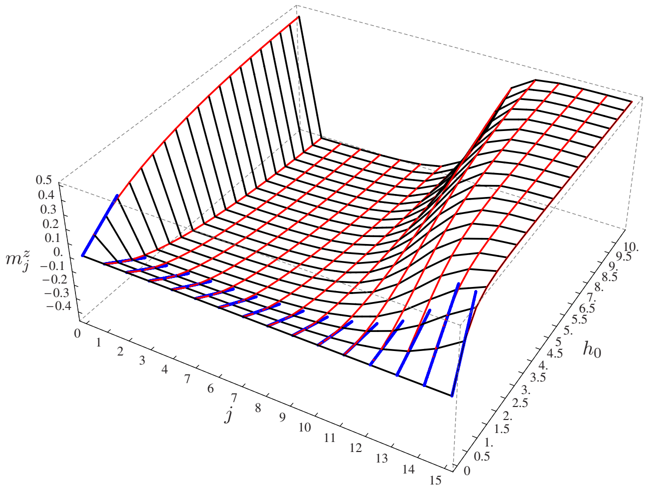

FIG. 3. (Color online) Magnetization profiles as a function of the site j and the central field h_0 for $S^z_{\mathrm{tot}}=0$ with the couplings, Eq. (2), where $x_1=2$ and $B=2$, obtained by inserting the numerical solution of Eqs. (41) and (40) for δ,ν into Eqs. (38) and (39) for m_j^z. The short heavy (blue) lines in the foreground denote the leading contribution for small fields and large particle number, Eqs. (55) and (56).

In Fig. 4 we compare the diagonalization results with the full classical expressions, Eqs. (38) and (39), and with the approximate results, Eqs. (55) and (56), for three different values of h_0. The small-field expansion in Eq. (56) deviates from the exact data essentially at large distances from the center of the dot, where the more weakly bound spins are located. On the other hand, Eq. (39) with values for δ,ν obtained by solving Eqs. (40) and (41) numerically deviates from the exact solution only by a few percent or less. Comparing the classical expression for the two-point function Eq. (43) with the diagonalization results, one notices considerable differences, see Fig. 5.

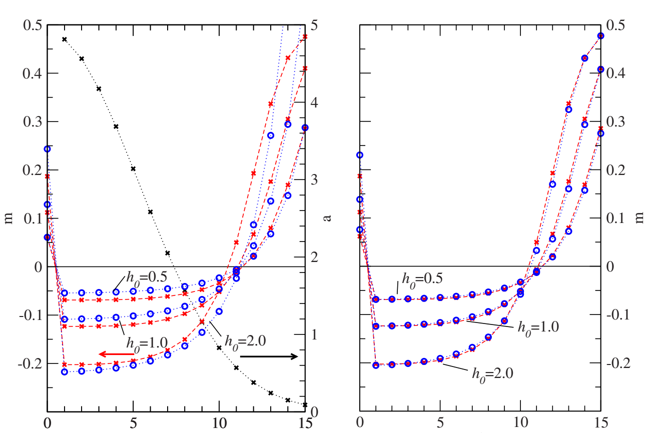

FIG. 4. (Color online) The local magnetization $\langle S_j^z\rangle_0$ obtained for a $N=16$-spin system with couplings as in Fig. 1. The central field assumes values $h_0=0.5$, 1, and 2, as indicated in the figure. The total polarization is fixed at $S^z_{\mathrm{tot}}=0$. Data from complete diagonalization (red crosses) are compared to the small-field expressions Eqs. (55) and (56) (green diamonds) and the mean-field result Eq. (39) (blue circles), where δ,ν were obtained by numerically solving Eqs. (40) and (41).

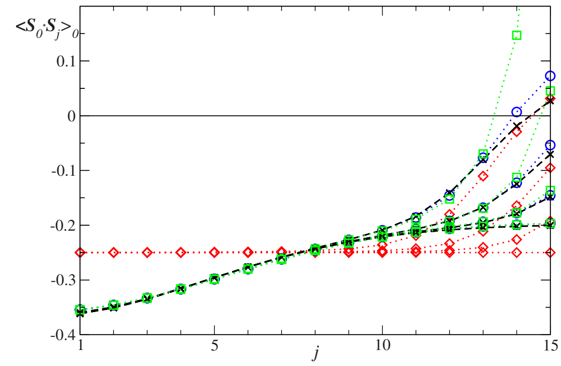

FIG. 5. (Color online) Two-point function $\langle \boldsymbol{S}_0\cdot\boldsymbol{S}_j\rangle_0$ in the ground state for the model with the same exchange couplings chosen as in Fig. 1 and central field values $h_0=0,0.5,1.0,2.0$ (bottom to top). Black crosses were computed from a complete diagonalization. Red diamonds stem from the purely classical solution, Eq. (43). In later sections, quantum contributions are calculated. Green squares were obtained from Eq. (94), where the leading finite-size quantum effects are included. Blue circles are based on Eq. (111), where classical and quantum contributions are summed.

IV. CORRELATION FUNCTIONS FROM THE EXACT QUANTUM-MECHANICAL SOLUTION

Whereas in the previous section a classical picture of the central spin model was sketched, this section contains a systematic study of the exact quantum-mechanical solution, where the contribution of quantum fluctuations to the correlation functions will be emphasized. We will first obtain approximate analytical expressions for correlation functions in the regimes of zero and weak central magnetic fields, before recovering the classical picture from the previous section in the appropriate limit.

A. No field

For vanishing magnetic field, the Hamiltonian (1) is SU(2) invariant and commutes with all components of the total spin, $[H|_{h=0},\boldsymbol{S}_{\mathrm{tot}}]=0$. In other words, all states within one spin multiplet, obtained by acting with $S^{\pm}_{\mathrm{tot}}$ on highest weight states, are energetically degenerate. In the expression for the eigenstates Eq. (7), application of S^-_{tot} corresponds to fixing one of the Bethe-Ansatz numbers at $\omega_k=0$. Indeed, for $h_0=0$, it is easy to see that if $\{\omega_1,\ldots,\omega_M\}$ is a solution of the coupled set of Eqs. (6), then $\{\omega_1,\ldots,\omega_M,0\}$ is a solution as well. Both these solutions are energetically degenerate, according to Eq. (5). This situation is analogous to the Heisenberg chain, where sets of only finite Bethe roots encode the highest weight states.[46,47] Here and in the following, the ground-state energy and expectation values in the ground state will be labeled by the subscript 0.

1. Ground state

The ground state maximizes $\sum_{k=0}^{M_b}\omega_k$. It turns out that the corresponding highest weight state has $M_b=0$ so that only one Bethe number ω_0 has to be determined from $1-\sum_{j=1}^{N_b}\frac{A_j}{\omega_0-A_j}=0$. We are interested in the energy levels for large particle numbers. In the ground state, $\omega_0=\mathcal{O}(N)$, which allows us to rewrite the single BAE in terms of the moments x_n defined in Eq. (51)

$$1 - N_b \sum_{n=1}^{\infty} \frac{x_n}{\omega_0^n} = 0. \tag{57}$$

We define $\omega_0 =: \tilde{\omega}_0 N_b$, such that both x_n and $\tilde{\omega}_0$ are $\mathcal{O}(1)$. Then, according to Eq. (5), the ground-state energy reads

$$E_0 = -\frac{N_b}{2}\left(\tilde{\omega}_0 - \frac{x_1}{2}\right) \tag{58}$$

and successive orders of $\tilde{\omega}_0$ in an asymptotic expansion for large particle numbers can be obtained by inverting Eq. (57) order by order. Let $\tilde{\omega}_0^{(n)}$ be the expansion of $\tilde{\omega}_0$ in powers of N_b^{-1} up to order n, i.e., $\lim_{N_b\to\infty}(\tilde{\omega}_0 - \tilde{\omega}_0^{(n)})N_b^{n+1} = \mathcal{O}(1)$. For $n=3$, with $d := (N_b x_1)^{-1}$ and $y_n := x_{n+1}/x_1$, we obtain

$$\frac{\tilde{\omega}_0^{(3)}}{x_1} = 1 + y_1 d + (-y_1^2 + y_2)d^2 + (2y_1^3 - 3y_1 y_2 + y_3)d^3. \tag{59}$$

This leads us to conjecture that the coefficient of d^n in the expansion of $(\tilde{\omega}_0/x_1 - 1)$ is given by the nth coefficient in a Taylor expansion of $n!\ \ln[\phi(d)/x_1]$ in the variable d, where the generating function is $\phi(d) = \sum_{j=1}^{N_b} A_j \exp[dA_j]/N_b$.

Before continuing, let us make two comments on Eq. (59): to begin with the leading term, when plugged into Eq. (58), yields the overall ground-state energy of the classical model in Eq. (27) with no fields, where the central spin is pointing in the direction opposite to the nuclear bath spins. Finite-size corrections, given by the subleading terms in Eq. (59) therefore represent quantum effects. Secondly, for the homogeneous model $A_j \equiv A\,\forall j$, all but the first two terms on the right-hand side of Eq. (59) vanish.

It is now straight forward to evaluate the moments for a given distribution of the coupling constants A_j. For the particular case of the choice in Eq. (2) it is possible to use the Euler MacLaurin summation formula to find an expansion of the moments in the parameter d. Writing $y_1 = y_1^{(0)} + d y_1^{(1)}$, we find

$$y_1^{(0)} = 2x_1 \frac{B\ \mathrm{Erf}(\sqrt{2}B)}{\sqrt{2\pi}\ \mathrm{Erf}^2(B)}, \tag{60}$$

$$y_1^{(1)} = -\frac{2x_1^2 B^2}{\pi \mathrm{Erf}^2(2)} + 4B^2 \frac{\mathrm{Erf}(\sqrt{2}B)}{\pi\sqrt{2}\mathrm{Erf}^3(B)}. \tag{61}$$

Therefore, the coefficient of d^2 in Eq. (59) becomes

$$[-(y_1^{(0)})^2 + y_2^{(0)}] = \frac{2x_1^2 B^2}{\pi \mathrm{Erf}^3(2)}[-\mathrm{Erf}^2(\sqrt{2}B)/\mathrm{Erf}(B) + 2\mathrm{Erf}(\sqrt{3}B)/\sqrt{3}]. \tag{62}$$

As expected, this latter expression tends to zero for $B \to 0$, which is the homogeneous limit in the couplings in Eq. (2).

From Eq. (58), one then obtains for the ground-state energy

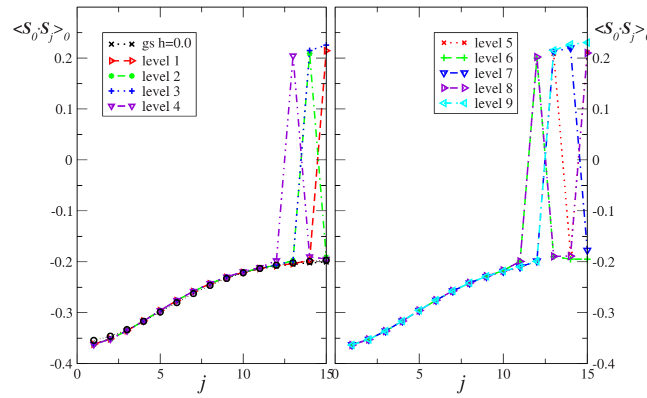

FIG. 6. (Color online) The two-point function $\langle \boldsymbol{S}_0 \cdot \boldsymbol{S}_j \rangle$ for zero magnetic field in the gs and the lowest ten excited levels (couplings as in Fig. 4), obtained from complete diagonalization. The circles in the left panel are the analytical result Eq. (64) for the ground state.

$$E_0 = -\frac{1}{4d} - \frac{y_1^{(0)}}{2} - \frac{d}{2}[y_1^{(1)} - (y_1^{(0)})^2 + y_2^{(0)}]. \tag{63}$$

The first term is the classical result, where the central spin is aligned antiferromagnetically with respect to the bath spins. The second and third terms constitute quantum corrections.

In order to calculate the two-point correlation function $\langle \boldsymbol{S}_0 \cdot \boldsymbol{S}_j \rangle_0$ in the ground state, one combines Eq. (8) with Eq. (63). This yields up to order d

$$\langle \boldsymbol{S}_0 \cdot \boldsymbol{S}_j \rangle_0 = -\frac{1}{4} + \frac{d}{2} y_1^{(0)} - dA_j. \tag{64}$$

Again, the leading contribution reflects the classical picture of antiferromagnetically aligned spins. For zero central field, quantum fluctuations lead to a nontrivial dependence on the distance j between the bath and the central spins. This is a pure quantum effect as can be seen by comparison with Eq. (54). Especially, quantum fluctuations decrease $\langle \boldsymbol{S}_0 \cdot \boldsymbol{S}_j \rangle_0$ below the classical result $-1/4$ if $A_j > y_1^{(0)}/2$, i.e., for the strongly coupled bath spins. In Fig. 6 the result in Eq. (64) is compared to complete diagonalization data. In the homogeneous case $A_j = A\,\forall j$, Eq. (64) reduces to the result found in Refs. 48 and 49.

To calculate the magnetization profile $\langle S_j^z \rangle_0$, we can employ Eq. (20) together with Eq. (59). Let us first consider the case of a fully polarized bath. For $S_{\mathrm{tot}}^z = N/2 - 1$, in leading order this leads to

$$\langle S_j^z \rangle_0 = \frac{1}{2} - d^2 A_j^2, \quad j = 1, \ldots, N_b, \tag{65}$$

$$\langle S_0^z \rangle_0 = -\frac{1}{2} + d y_1^{(0)}. \tag{66}$$

At smaller values for S_{tot}^z, we can still use Eq. (20), keeping in mind that it has been derived at finite h_0. We thus have to perform the derivative in Eq. (20) before taking the limit $h_0 \to 0$. In this limit, the eigenvalues $\tilde{\Lambda}$ in Eq. (19) were given in Ref. 50, Eq. (39). Using that result we obtain the

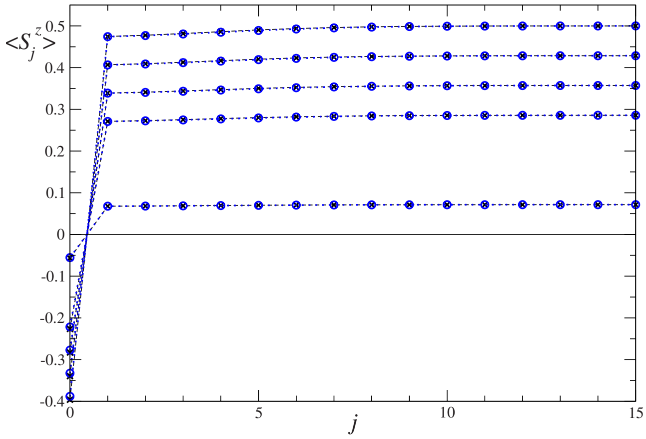

FIG. 7. (Color online) The local magnetization $\langle S_j^z \rangle$ for $N_b=15$ bath spins with the couplings, Eq. (2), where $x_1=2$ and $B=2$. Black crosses stem from a complete diagonalization, blue circles (mostly containing crosses) from Eq. (67). For the central spin, $\langle S_0^z \rangle$ was determined such that S_{tot}^z is fixed, which in leading order is given by Eq. (68). From top to bottom, $S_{\text{tot}}^z=7,6,5,4,1$.

expectation values in the respective ground state of each sector S_{tot}^z

$$\langle S_j^z \rangle_0 = \frac{S_{\text{tot}}^z}{N-2}(1-2d^2A_j^2), \quad j=1,\ldots,N_b, \tag{67}$$

$$\langle S_0^z \rangle_0 = \frac{S_{\text{tot}}^z}{N-2}(-1+2dy_1^{(0)}). \tag{68}$$

For $S_{\text{tot}}^z=N/2-1$, Eqs. (65) and (66) are recovered. In the opposite limit, $S_0^z=0$, the polarization vanishes, as expected from the SU(2) invariance in this case. In Fig. 7, we compare the analytical results, Eqs. (67) and (68), with complete diagonalization data. These illustrate the fact that the magnetization profiles are different for energetically degenerate states.

2. Excited states

In the classical picture, the lowest excitations at $h_0=0$ above the Néel-type ground state are created by flipping the spins in the outer region where the exchange with the central spin is weakest. In the exact solution of the quantum-mechanical problem, Eqs. (5) and (6), excitations can be of two types: (i) spin excitations with a change in M, i.e., the number of roots. (ii) Particle-hole excitations, where the location of roots is changed with respect to the ground state but the number of roots is kept fixed.

For $h_0=0$, both types of excitations are energetically equivalent: adding a root $\omega_k \neq 0$ is equivalent to moving a root $\omega_k=0$ to a finite value. Let us consider an excited state with M_b+1 nonzero roots. We focus on low-lying excitations here, so $M_b \ll N$. The ground state with the same M_b value, i.e., with $2S_{\text{tot}}^z=N-2(M_b+1)$, has one nonzero root and M_b roots at zero. Moving these roots away from zero leads to the excited state of interest here. In the Bethe-Ansatz Eq. (6), there is one root which scales like the particle number; we denote it by ω_0, i.e. $\omega_0=\mathcal{O}(N)$. The M_b additional roots are smaller, $\omega_k=\mathcal{O}(1)$.

We define the moments of the additional nonzero roots as $\gamma_n := \sum_{k=1}^{M_b}\omega_k^n$. Performing an expansion analogous to Eq. (57), one obtains for the root $\omega_0=\mathcal{O}(N)$ the equation

$$1 - N_b\sum_{n=1}^{\infty}\frac{x_n}{\omega_0^n} + 2\sum_{n=1}^{\infty}\frac{\gamma_n}{\omega_0^n} = 0, \tag{69}$$

which again can be inverted order by order. Including terms of order $\mathcal{O}(1/N_b)$

$$\omega_0 = \frac{1}{d} - 2\gamma_1 + y_1 + 2dy_1\gamma_1 - 2d\gamma_2 + d(y_2 - y_1^2). \tag{70}$$

This leads to an expression for the energy in terms of the γ_n

$$E_{\text{ex}} = -\frac{1}{4d} + \gamma_1 - \frac{y_1^{(0)}}{2} - \frac{d}{2}[2y_1^{(0)}\gamma_1 + 2\gamma_2 + y_1^{(1)} - (y_1^{(0)})^2 + y_2^{(0)}]. \tag{71}$$

Let us look at the simplest case, $M_b=1$. The corresponding equation for the additional root ω_1 reads

$$1 - \sum_{j=1}^{N_b}\frac{A_j}{A_j-\omega_1} + 2\frac{\omega_1}{\omega_0} + 2\frac{\omega_1^2}{\omega_0^2} = 0. \tag{72}$$

By sketching the lhs of this equation, one sees that ω_1 is located between two couplings. Indeed, for the lowest excitation, we can set $\omega_1=A_{N_b}+\delta_{N_b}$. Thus ω_1 lies between the two smallest couplings A_{N_b} and A_{N_b-1}, and the most weakly coupled spin is flipped. In leading order, we then obtain $\delta_{N_b}=A_{N_b}/[\sum_{j=1}^{N_b-1}A_j/(A_j-A_{N_b})-1]=\mathcal{O}(1/N_b)$ and $\delta_{N_b}>0$. One can generalize this result to $\omega_1=A_\ell+\delta_\ell$ as long as $\delta_\ell=\mathcal{O}(1/N_b)$ and $\delta_\ell>0$, i.e., for $\ell \geqslant 1$. Then Eq. (64) is modified according to

$$\langle \boldsymbol{S}_0 \cdot \boldsymbol{S}_j \rangle_{\text{ex}} = \begin{cases} -\frac{1}{4} + \frac{d}{2}y_1^{(0)} - dA_j, & j \neq \ell, \\ \frac{1}{4} - \frac{d}{2}y_1^{(0)} + dA_j, & j = \ell. \end{cases} \tag{73}$$

This corresponds to the classical picture of a single spin flip with respect to the ground state close to the outer edges of the quantum dot where the coupling is smallest. That result generalizes further to the case of more than one excitation, $M_b>1$. If more than one BA root is present, different root patterns are possible. Let us call the distance A_j-A_{j+1} the jth coupling interval. We call an interval occupied if one root is located within this interval.

One type of root configurations consists of only real roots and occupied intervals with no consecutive occupied intervals. Another type of root configurations involves consecutive occupied intervals. However, depending on the special choice of the coupling constants and the central magnetic field, roots in such a configuration can be driven into the complex plane, thus forming complex-conjugate pairs.[39,51,52]

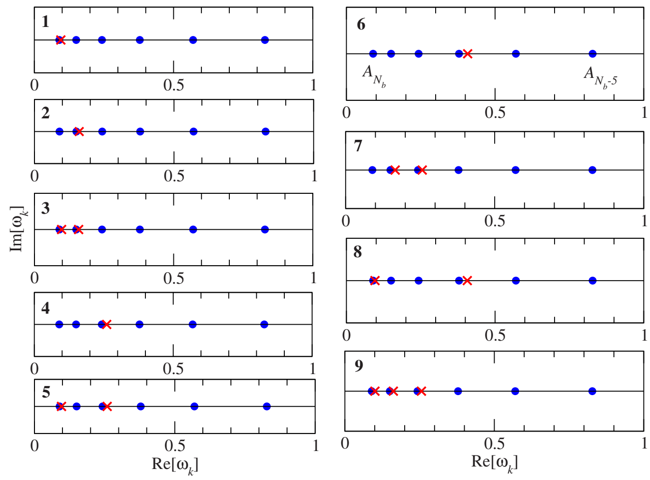

FIG. 8. (Color online) The location of the additional BA numbers which are $\mathcal{O}(1)$ (red crosses) for the lowest nine excitations (top left: level 1 and bottom left: level 5) with $N_b=15$, $x_1=2$, and $B=2$ in Eq. (2) for the couplings. The six smallest couplings are shown here (blue dots). Not shown is $\omega_0=\mathcal{O}(N_b)$.

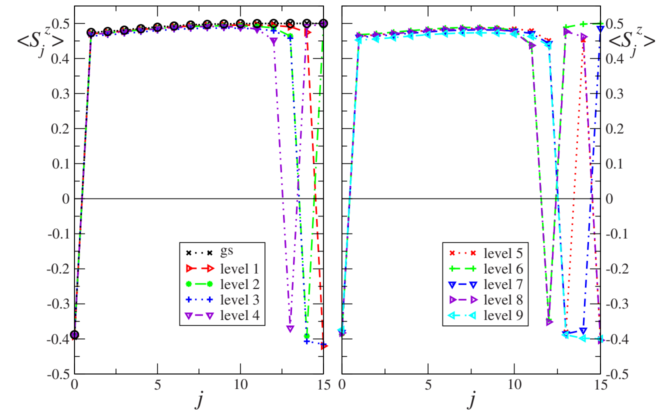

FIG. 9. (Color online) The magnetization profile $\langle S_j^z\rangle_{\text{ex}}$ in the ground state and the lowest nine excited levels corresponding to the root configurations of Fig. 8, obtained from complete diagonalization. The circles for the ground state in the left panel are the analytical results from Eq. (67). The analogous excited-state result Eq. (74) is not shown since it can be obtained by simply changing the sign of $\langle S_j^z\rangle$ for $j=\ell_1,\ldots,\ell_n$ where $\ell_1,\ldots,\ell_n$ are the quantum numbers of the excited state.

From these observations we conclude that the two-point function $\langle \boldsymbol{S}_0\cdot\boldsymbol{S}_j\rangle_{\text{ex}}$ yields significant insight into the underlying root configuration of a low-lying excited state. *Vice versa*, if the root configuration for low-lying excitations is known, the corresponding two-point function can be predicted at least qualitatively. This prediction confirms nicely the physical expectation.

In Fig. 6, we depict $\langle \boldsymbol{S}_0\cdot\boldsymbol{S}_j\rangle_{\text{ex}}$ for the lowest nine excited states for $N=16$ particles with the couplings chosen according to Eq. (2) with $x_1=2$ and $B=2$. The data have been obtained from complete diagonalization. The analytical result, Eq. (64), for the ground state is given as well, from which the analytical predictions for excited states are obtained straightforwardly by changing the sign of the corresponding spins, like in Eq. (73).

It is instructive to consider the corresponding root configurations of those lowest nine excited levels. These are shown in Fig. 8 for the highest weight states, i.e., without roots in the origin. The physical interpretation of the root locations as spin flips with respect to the ground state is revealed when comparing the root pattern level by level with the j dependence of the two-point function.

This interpretation carries over to the magnetization profile. We show those magnetization profiles corresponding to the lowest nine excited levels in Fig. 9. However, as in the ground state, an important difference consists in the degeneracy of $\langle \boldsymbol{S}_0\cdot\boldsymbol{S}_j\rangle_{\text{ex}}$ for all states within one multiplet. Whereas the two-point function is independent of the total magnetization S_{tot}^z, the local magnetization $\langle S_j^z\rangle_{\text{ex}}$ does depend on that quantity. In Fig. 9, we only give the magnetization profiles for the highest weight states parametrized by the roots sketched in Fig. 8. By adding additional roots in the origin, i.e., by lowering S_{tot}^z, the two-point function is not altered but $\langle S_j^z\rangle_{\text{ex}}$ is changed by an overall prefactor like in Eqs. (67) and (68). Namely, proceeding similarly as in the derivation of Eqs. (67) and (68), one obtains the leading terms of the magnetization profile in low-lying excited states

$$\langle S_j^z\rangle_{\text{ex}} = \begin{cases} \dfrac{S_{\text{tot}}^z}{N-2n}(1-2d^2A_j^2), & j\neq \ell_1,\ldots,\ell_n, \\ -\dfrac{S_{\text{tot}}^z}{N-2n}(1-2d^2A_j^2), & j=0,\ell_1,\ldots,\ell_n. \end{cases} \tag{74}$$

Here $n\geq 1$ is the number of nonzero roots and the indices $\ell_1\ldots\ell_n$ denote their locations relative to the couplings. For low-lying states, the roots are located close to the couplings $A_{\ell_1},\ldots,A_{\ell_n}$, as can be seen from Fig. 8. All states with the same n but different S_{tot}^z are energetically degenerate, i.e., have identical two-point functions $\langle \boldsymbol{S}_0\cdot\boldsymbol{S}_j\rangle_{\text{ex}}$ but different magnetization profiles $\langle S_j^z\rangle_{\text{ex}}$. For the highest weight states we have $S_{\text{tot}}^z=N/2-n$, which is also the case for the root configurations depicted in Fig. 8. According to Eq. (74) the magnetization profile therefore can be read off from the number and location of Bethe roots. This is confirmed by complete diagonalization data shown in Fig. 9. Deviations from Eq. (74) are due to interactions between the excitations, which were neglected in the derivation of Eq. (74).

B. Weak field

A finite magnetic field couples to both the electronic and nuclear spins. As described after Eq. (4), the coupling to the nuclear spins is trivial and can be accounted for at the end of the calculation. Let us thus first focus on $h_0\gtrsim 0$ and $h_t=0$. As stated in the previous section, for $h_0=0$, the eigenvalues of a given multiplet are degenerate, which in the root pattern is encoded by roots in the origin. For $h_0\neq 0$, this degeneracy is lifted due to the broken SU(2) invariance. Thus it is reasonable to assume that the zero roots are driven away from the origin by a finite magnetic field h_0. In the weak-field limit, this is confirmed by the large-g expansion of the Bethe roots[50] of the BCS Hamiltonian (25), which are related to the

Bethe roots of the central spin model via Eq. (16). In this section, we will derive the energy eigenvalues and expressions for the screening cloud and magnetization profile for small but finite central field.

1. Ground state

Starting from Eq. (6), we include a finite field h_0 in Eq. (69). We then arrive at the following equations for $\omega_{k=0,\ldots,N_b}$:

$$1 - N_b\sum_{n=1}^{\infty}\frac{x_n}{\omega_0^n} + 2\sum_{n=1}^{\infty}\frac{\gamma_n}{\omega_0^n} + \frac{2h_0}{\omega_0} = 0, \tag{75}$$

$$1 + \sum_{j=1}^{N_b}\frac{A_j}{A_j-\omega_k} - 2\sum_{n=0}^{\infty}\left(\frac{\omega_k}{\omega_0}\right)^n - 2\sum_{\substack{k'=1\\k\neq k'}}^{M_b}\frac{\omega_{k'}}{\omega_{k'}-\omega_k} + \frac{2h_0}{\omega_k} = 0. \tag{76}$$

Thus the only effect of h_0 in Eq. (75) compared to Eq. (69) is to add a term $-2h_0$ to $N_b x_1$, i.e., up to order $\mathcal{O}(1/N_b)$ we have

$$\omega_0 = N_b x_1 - 2h_0 - 2\gamma_1(1-dy_1) + y_1(1+2h_0 d) - 2\gamma_2 d + d(y_2 - y_1^2). \tag{77}$$

One then obtains for the ground-state energy an expression which still involves the M_b nonzero roots

$$E_0 = -\frac{1}{4d} + \frac{h_0}{2} + \frac{\gamma_1}{2} - \frac{y_1}{2} - \frac{d}{2}[y_2 - y_1^2 + h_0 y_1 + y_1\gamma_1 - \gamma_2]. \tag{78}$$

Let us now multiply Eq. (76) by ω_k and sum all terms $k=1,\ldots,M_b$. We assume that h_0 is sufficiently small so that $\max\{|\omega_k|\} < A_{N_b}$ and find

$$\gamma_1 + 2\sum_{j=2}^{\infty}\frac{\gamma_j}{\omega_0^{j-1}} = N_b\sum_{j=1}^{\infty}x_{-j}\gamma_{j+1} \tag{79}$$

with $x_0 \equiv 1$. Here, we aim at calculating the energy up to $\mathcal{O}(h_0^2)$. In analogy to Ref. 50, we therefore make the Ansatz

$$\gamma_1 = c_1 h_0 + c_2 h_0^2 + \mathcal{O}(h_0^3), \tag{80}$$

$$\gamma_2 = d_1 h_0^2 + \mathcal{O}(h_0^3). \tag{81}$$

Then, including terms $\mathcal{O}(h_0^2)$, the coefficients $c_{1,2}$ are found by inserting that Ansatz into Eq. (79)

$$c_1 = -\frac{2M_b}{N_b - 1}, \tag{82}$$

$$c_2 = \frac{1}{N_b-1}(2d - x_{-1})d_1 = -\frac{x_{-1}}{N_b-1}d_1 + \mathcal{O}(d^2), \tag{83}$$

where we only keep the leading finite-size terms.

An additional equation is thus needed to determine d_1. This is obtained by adapting the techniques used in Ref. 50 to our problem. We then find that in leading order in h_0, the roots $\omega_{k=1,\ldots,M_b}$ are related to the zeros of associated Legendre polynomials

$$L_{M_b}^{-N_b}\left(\frac{2h_0}{\omega_k}\right) = 0. \tag{84}$$

This is a polynomial of degree M_b, i.e., $L_{M_b}^{-N_b}(x) \equiv c\prod_{k=1}^{M_b}(x - 2h_0/\omega_k)$, where the constant c is determined by the asymptotes. Consequently, the logarithmic derivative at $x=0$ is

$$[\ln L_{M_b}^{-N_b}(x)]'|_{x=0} = -\frac{\gamma_1}{2h_0}. \tag{85}$$

On the other hand, $[\ln L_{M_b}^{-N_b}(x)]'|_{x=0} = M_b/(N_b-1)$, which in combination with Eq. (85) confirms Eq. (82). Analogously, the second logarithmic derivative $[\ln L_{M_b}^{-N_b}(x)]''|_{x=0} = M_b(M_b + 1 - N_b)/[(N_b-2)(N_b-1)^2]$, which leads to

$$\frac{M_b(M_b+1-N_b)}{(N_b-2)(N_b-1)^2} = -\frac{\gamma_2}{(2h_0)^2}. \tag{86}$$

Combining this equation with Eq. (81), one finds in terms of S_{tot}^z

$$d_1 = \frac{(N_b-1)^2 - 4(S_{\mathrm{tot}}^z)^2}{(N_b-2)(N_b-1)^2}, \tag{87}$$

$$c_2 = -x_{-1}\frac{(N_b-1)^2 - 4(S_{\mathrm{tot}}^z)^2}{(N_b-2)(N_b-1)^3}N_b, \tag{88}$$

where the latter relation follows from Eq. (83). Then the ground-state energy reads

$$E_0 = -\frac{1}{4d} - \frac{y_1}{2} + \frac{S_{\mathrm{tot}}^z}{N_b-1}h_0 - 2\frac{S_{\mathrm{tot}}^z}{N_b-1}dy_1h_0 + \frac{c_2}{2}h_0^2 - \frac{d}{2}(y_2 - y_1^2) + \mathcal{O}(d^2) \tag{89}$$

$$= -\frac{1}{4d} - \frac{y_1^{(0)}}{2} - \frac{d}{2}[y_1^{(1)} - (y_1^{(0)})^2 + y_2^{(0)}] + s_{\mathrm{tot}}^z h_0(1 - 2dy_1) - \frac{1 - 4(s_{\mathrm{tot}}^z)^2}{2N_b}x_{-1}^{(0)}h_0^2 + \mathcal{O}(d^2) \tag{90}$$

where we have defined the total magnetization density $s_{\mathrm{tot}}^z := S_{\mathrm{tot}}^z/(N_b-1)$. In the last equation, the leading orders in a finite-size and small-h_0 expansion are given. For $S_{\mathrm{tot}}^z=0$, the central magnetic field does not enter linearly but due to second-order spin-exchange processes only quadratically.

We now take into account the total field term $-h_{\mathrm{t}}S_{\mathrm{tot}}^z$ from Eq. (3). Adding that term to Eq. (90) and temporarily treating the fields h_0 and h_{t} as independent parameters creates an interesting pattern: for fixed h_{t} the lowest levels $E_0(S_{\mathrm{tot}}^z, h_0)$ display a pattern which is strongly reminiscent of light rays forming a caustic in optics. Figure 10 demonstrates that for a finite total magnetic field h_{t}, a small but finite range of values for h_0 exists where the state with $S_{\mathrm{tot}}^z=0$ is the ground state. Or, coming back to the original Hamiltonian (1), this means

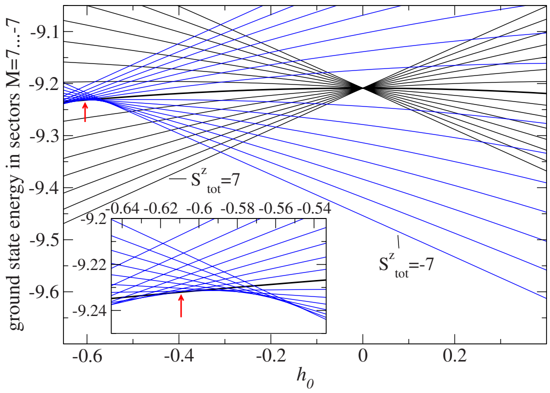

FIG. 10. (Color online) Lowest levels in the sectors $M=7,\ldots,-7$ for $N_b=15$ and couplings as in Eq. (2) with $x_1=B=2$, obtained from a numerical solution of Eq. (6). Black lines intersecting at $h_0=0$ (the fat black line is the energy for $S^z_{\rm tot}=0$) and blue lines forming a caustic near $h_0=-0.6$. The inset is a zoom into the region around the caustic. The red arrows mark h_0 values such that the state with $S^z_{\rm tot}=0$ is the ground state.

that for any finite ratio g_n/g_e and given h_t one can adjust the central field h_0 such that the ground state has a given magnetization $S^z_{\rm tot}$. For the example shown in Fig. 10, the ground state has zero magnetization for $h_t=-0.035$, $h_0\approx-0.61$, which corresponds to $g_n/g_e\approx0.054$ with $hg_n=h_t$.

To find the relation between h_0 and h_t for the lowest energy level with a given $S^z_{\rm tot}$ we have to study the function $E_0(h_t,S^z_{\rm tot})=E_0(S^z_{\rm tot})-h_tS^z_{\rm tot}$, where $E_0(S^z_{\rm tot})$ is given by Eq. (90). Since $E_0(h_t,S^z_{\rm tot})$ is the Legendre transform of $E_0(S^z_{\rm tot})$, h_t can be calculated as $h_t=\partial_{S^z_{\rm tot}}E_0(S^z_{\rm tot})$ which leads to

$$h_t=\frac{h_0}{N_b-1}(1-2dy_1)+4S^z_{\rm tot}x_{-1}^{(0)}\left(\frac{h_0}{N_b-1}\right)^2 \qquad (91)$$

up to higher order corrections. For $S^z_{\rm tot}=0$, this is inverted to

$$h_0=(N_b-1)(1+2dy_1)h_t=\left(N_b+\frac{2x_2^{(0)}}{x_1^2}-1\right)h_t+\mathcal{O}(d), \qquad (92)$$

which for the numerical values chosen in Fig. 10 yields $h_0\approx-0.60$, in good agreement with the exact numerical data from the Bethe Ansatz. From the classical Hamiltonian (53), only the leading contribution in the particle number in Eq. (92) is recovered. From Eq. (92), the ratio of g factors in the $S^z_{\rm tot}=0$ sector is deduced (setting $hg_n=h_t$)

$$\frac{g_e}{g_n}=N_b+\frac{2x_2^{(0)}}{x_1^2}+\mathcal{O}(d). \qquad (93)$$

This means that when the ratio of electronic to nuclear g factors equals the number of nuclear bath spins then an overall magnetic field drives the system into the nondegenerate $S^z_{\rm tot}=0$ state.

Let us now consider correlation functions. From Eq. (8), we obtain for large particle numbers

$$\langle \boldsymbol{S}_0\cdot\boldsymbol{S}_j\rangle_0=-\frac{1}{4}+\frac{d}{2}y_1-dA_j-\frac{d^2}{2}(-2y_2+3y_1^2+3A_j^2-4y_1A_j)+\frac{c_2^{(0)}}{2}\frac{h_0^2}{A_j^2}+\mathcal{O}(d^3) \qquad (94)$$

with $c_2^{(0)}=[1-4(s^z_{\rm tot})^2]/N_b^2$. If one is interested in the coefficients of the asymptotic $1/N_b$ expansion one should again apply the Euler-MacLaurin formula as in Eq. (63). We do not want to dwell into these technical but straightforward details here but rather compare the analytical prediction with exact results from complete diagonalization. Such a comparison is shown in Fig. 5 in Sec. III D.

As expected, the approximation, Eq. (94), is reliable quantitatively only for small fields, according to our weak-field assumption $\max\{|\omega_k|\}<A_{N_b}$. From Eq. (80), one estimates $|\omega_k|\approx2h_0/N_b$, which means that Eqs. (90) and (94) are valid for $|h_0|\lesssim A_{N_b}N_b/2$. For our choice of parameters $N_b=15$ and $x_1=B=2$ in the complete diagonalization of Eq. (2), this means $|h_0|\lesssim0.7$. But even for larger values of h_0, Eq. (94) is qualitatively correct: a finite central magnetic field leads to an enhanced *ferromagnetic* correlation between the central spin and the rather loosely bound bath spins at larger distances from the center of the dot, and to an enhanced *antiferromagnetic* correlation between the central spin and the bath spins closer to the center of the dot, which is also consistent with the classical magnetization profile in Fig. 3.

We also want to compare Eq. (94) with Eq. (54), obtained within the classical picture for $S^z_{\rm tot}=0$ for $h_0\gtrsim0$. In that approximation, the equations differ from each other by field-independent terms proportional to d. This is understandable: we have seen in Eq. (64) that these terms constitute finite-size corrections which stem from quantum fluctuations and are thus not present within the classical approach. These lead to an increase in the amplitude of two-point functions. Especially, for the stronger couplings, values smaller than the classical bound $-1/4$ are reached, a clear sign of entanglement and noncommutativity of the quantum spin operators.

In order to determine quantum fluctuations to $\langle S_j^z\rangle$ in the small-field limit, one has to solve the set of Eqs. (18) for the E_j in order to determine the eigenvalue in Eq. (19). From this, the local magnetization is obtained via Eq. (20).

The small-field expansion of the set of Eqs. (18) has been studied in detail in Ref. 50. From that work, it follows that for the ground state of the central spin model at fixed N_b and M_b

$$\sum_{k=1}^{N_b}E_k=E_{\rm gr}(M_b,N_b-1,\{x_{-p}-2E_0^p/N_b\}), \qquad (95)$$

where the integer $p>0$ and with

$$E_{\rm gr}(M_b,N_b-1,\{x_{-p}\})=-\frac{M_b(N_b-M_b)}{2h_0}+\frac{M_bN_bx_{-1}}{N_b-1}-2h_0(x_{-2}-x_{-1}^2)\frac{N_bM_b(N_b-1-M_b)}{(N_b-1)^2(N_b-2)}+\mathcal{O}(h_0^2). \qquad (96)$$

From Eq. (77) one computes

$$E_0 = d(1 + 2dh_0 + 2d\gamma_1 + dy_1) + \mathcal{O}(h_0^2, d^3) \tag{97}$$

and γ_1 follows from combining Eqs. (80) and (82). In linear order in h_0 and including orders $\mathcal{O}(d^3)$, one then obtains the magnetization profile

$$\langle S_j^z\rangle = s_{\text{tot}}^z[1 - 2A_j^2 d^2 - 16h_0 A_j^2 d^3 s_{\text{tot}}^z + A_j^2 d^3(3y_1 - 2A_j)] + [A_j^{-1} - x_{-1}(1 - 2d^2A_j^2) + 2d^2 x_1(1 - 2d^2 A_j^2)]\frac{1 - 4(s_{\text{tot}}^z)^2}{N_b - 2}h_0 \tag{98}$$

with $s_{\text{tot}}^z := S_{\text{tot}}^z/(N_b - 1)$. The polarization of the central spin, $\langle S_0^z\rangle$, is fixed by the sum rule $S_{\text{tot}}^z = \Sigma_{j=0}^{N_b}\langle S_j^z\rangle$. Comparing Eq. (98) with Eqs. (55) and (56), one again recognizes the effect of quantum fluctuations which are now subleading with respect to the classical contributions. As expected, these reduce the amplitude of the magnetization profile, signaling the effects of entanglement.

2. Excited states

In Sec. IV A 2, we found excitations for $h_0 = 0$. We can proceed similarly for $h_0 \gtrsim 0$. The expression (78) for the energy is still valid but the $\gamma_{1,2}$ are different now. Let us first consider single-particle excitations, parametrized by a single root ω_1 located on the real axis between A_{j+1} and A_j. Instead of Eq. (76) for $k = 1, \ldots, M_b$, the corresponding set of equations now reads

$$1 + \sum_{j=1}^{N_b} \frac{A_j}{A_j - \omega_1} - 2\sum_{j=0}^{\infty}\left(\frac{\omega_1}{\omega_0}\right)^j - 2\sum_{j=1}^{\infty}\frac{\gamma_j}{\omega_1^j} + \frac{2h_0}{\omega_1} = 0, \tag{99}$$

$$1 + N_b\sum_{j=0}^{\infty}\omega_k^j x_{-j} - 2\sum_{j=0}^{\infty}\left(\frac{\omega_k}{\omega_0}\right)^j - 2\sum_{j=0}^{\infty}\left(\frac{\omega_k}{\omega_1}\right)^j - 2\sum_{k'=2}^{M_b}\frac{\omega_{k'}}{\omega_{k'} - \omega_k} + \frac{2h_0}{\omega_k} = 0, \quad k = 2, \ldots, M_b. \tag{100}$$

By multiplying the latter equation with ω_k and taking the sum $k = 2, \ldots, M_b$, one arrives at an equation similar to Eq. (79) with $M_b \to M_b - 1$, $N_b \to N_b - 2$, and $x_{-n} \to x_{-n} - 2/(N_b\omega_1^n)$, $n = 0, 1, \ldots$. Thus the coefficients in Eqs. (80) and (81) are now

$$c_1^{\text{ex}} = -2\frac{M_b - 1}{N_b - 3}, \tag{101}$$

$$c_2^{\text{ex}} = \frac{1}{N_b - 3}\left(2d + \frac{2}{\omega_1} - N_b x_{-1}\right)d_1^{\text{ex}} \tag{102}$$

with $d_1^{\text{ex}} = d_1(N_b \to N_b - 2, S_{\text{tot}}^z \to S_{\text{tot}}^z)$ as defined in Eq. (87).

A small field does not change the root pattern of the lowest excited states qualitatively. Very similar to the discussion after Eq. (72), one can still make the Ansatz $\omega_\ell = A_\ell + \delta_\ell$ for single-particle excitations. Then for small h_0 and $\ell \gg 1$, one again finds that $\delta_\ell = \mathcal{O}(1/N_b)$. This picture carries over to multiparticle excitations, except that a finite field h_0 can lead to complex-conjugate pairs of roots.[39,51,52] Thus the low-energy excitations are still given by approximately independent spin flips of the outer bath spins. This is best seen when comparing the correlation functions $\langle \boldsymbol{S}_0 \cdot \boldsymbol{S}_j\rangle_{\text{ex}}$ and $\langle S_0^z\rangle_{\text{ex}}$ with the root patterns corresponding to the excited states. In Fig. 11, the two-point function $\langle \boldsymbol{S}_0 \cdot \boldsymbol{S}_j\rangle_{\text{ex}}$ is shown for the ground state and the lowest nine levels with a central field $h_0 = 1$ in the sector $S_{\text{tot}}^z = 0$. The corresponding magnetization profile, $\langle S_j^z\rangle_{\text{ex}}$ is sketched in Fig. 12, and Fig. 13 shows the underlying root patterns.

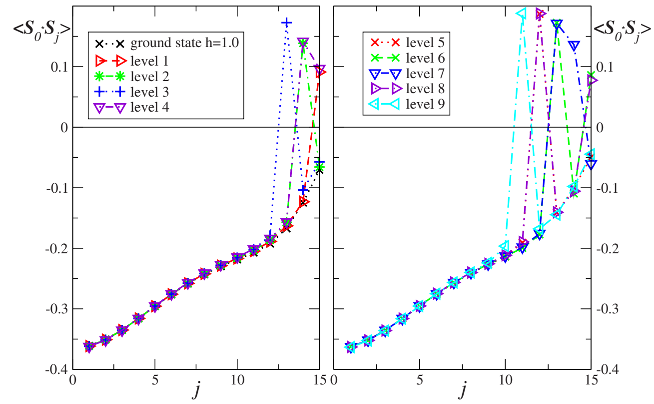

FIG. 11. (Color online) The two-point function $\langle \boldsymbol{S}_0 \cdot \boldsymbol{S}_j\rangle_{\text{ex}}$ for $h_0 = 1.0$ for the ground state and the lowest nine excited states, obtained from complete diagonalization with $N_b = 15$, and the couplings according to Eq. (2) with $x_1 = B = 2$.

Although qualitatively, the results are similar to those shown in Figs. 4 and 8, there are two important differences. First, the degeneracy between states within one multiplet is lifted so that both the one- and two-point functions depend on the total magnetization (in Figs. 11 and 12, we have chosen $S_{\text{tot}}^z = 0$). Second, the ordering of root configurations according to their energies is different. For example, the third excited level for $h_0 = 0$ is given by a two-particle excitation (two flipped spins) as shown in Fig. 8 whereas for $h_0 = 1.0$, such a configuration yields the fourth excited level, cf. Fig. 13.

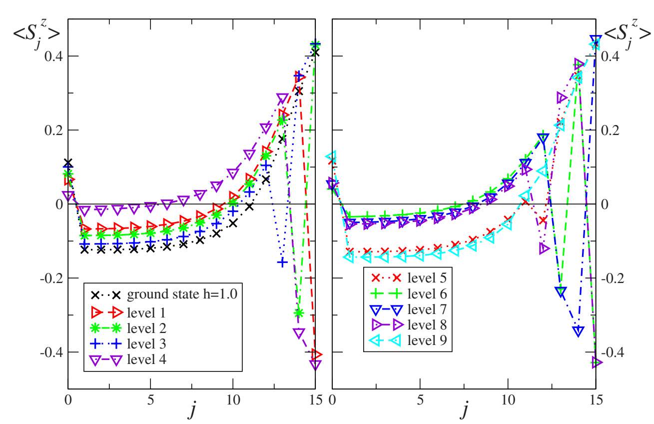

FIG. 12. (Color online) The magnetization profile for $h_0 = 1.0$ for the ground state and the lowest nine excited states, obtained from complete diagonalization with $N_b = 15$, and the couplings according to Eq. (2) with $x_1 = B = 2$.

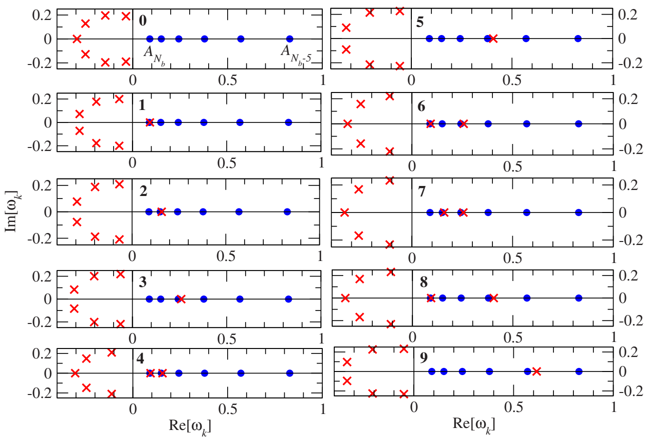

FIG. 13. (Color online) The location of those BA numbers which are $\mathcal{O}(1)$ (red crosses) in the complex plane for the ground state and the lowest nine excitations in the sector with $S^z_{\text{tot}}=0$ (top left: ground state and bottom left: level 4) with $N_b=15$, $x_1=2$, and $B=2$ in Eq. (2) for the couplings. The smallest six couplings are shown here (blue dots). Not shown is $\omega_0=\mathcal{O}(N_b)$.

C. From the exact solution to the classical picture

In this section, we want to make contact with the classical picture presented in Sec. III, starting from the exact solution for large N and small polarization, i.e., $M=\mathcal{O}(N)$, and finite central field. In this situation, the question arises whether the Bethe roots form a dense distribution in the complex plane, which would permit a continuum description. In Fig. 14, we show both the roots ω_k and their inverses $E_k=1/\omega_k$ for $N=16$, $M=8$, i.e., $S^z_{\text{tot}}=0$, parametrized by h_0. One can show[40] that for $g^{-1}=\mathcal{O}(N)$, the distribution of the E_k can be described by a cut in the complex plane in the thermodynamic limit $M,N\to\infty$, M/N fixed. However, for the central spin model, we are interested in $g^{-1}\equiv h_0=\mathcal{O}(1)$. Figure 14

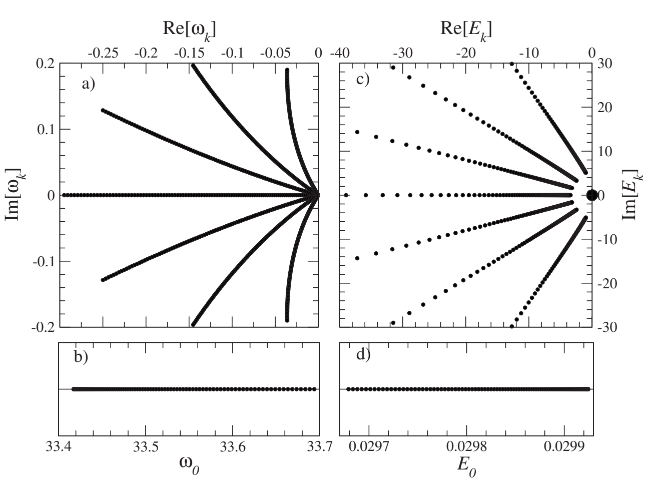

FIG. 14. (a) Bethe roots $\omega_k=\mathcal{O}(1)$ and $k=1,\ldots,7$ for $0<h_0\leq 1.0$. The field drives the roots away from the origin and the real root ω_0, shown in (b), moves towards the origin. (c) The inverse numbers $E_k\equiv 1/\omega_k$, including $k=0$ [on the real axis close to the origin (d) is a zoom showing E_0 only]. Here, the field makes the roots move towards the origin, except for E_0, which is shifted to larger real values.

suggests that such a continuum description still is possible in this case. To see this, we first review Richardson's[40] line of arguments for $g^{-1}\equiv\mathcal{O}(N)$.

Consider the function

$$F(z)=\sum_{k=0}^{M_b}\frac{1}{z-E_k}-\frac{1}{2}\sum_{j=0}^{N_b}\frac{1}{z-\varepsilon_j}-g^{-1}, \tag{103}$$

where ε_j, E_k are related to A_j, ω_k according to Eqs. (11) and (16) and $\varepsilon_0=0^-$. Then for $g^{-1}=\mathcal{O}(N)$, the function F is expanded as $F=F_0+F_1+\cdots$, where $F_\nu=\mathcal{O}(N^{-\nu+1})$. Such an expansion is justified rigorously by showing that F obeys a differential equation which can be solved order by order. We first consider the case where in the leading order, *all* E_k merge to form a cut in the complex plane along an arc which is symmetric with respect to the real axis. The endpoints of the arc, a and a^*, are parametrized by two real quantities, $a=\mu+i\Delta$, where μ and Δ are the chemical potential and the superconducting gap of the BCS model, Eq. (25). This situation corresponds to the ground state of the BCS model. Then

$$F_0(z)=-\sum_{j=0}^{N_b}\frac{\sqrt{(z-\mu)^2+\Delta^2}}{2(z-\varepsilon_j)\sqrt{(\varepsilon_j-\mu)^2+\Delta^2}}. \tag{104}$$

The ground state of the central spin model corresponds to a particle-hole excited state of the BCS model, where one root E_0 is taken away from the arc and instead is located on the positive real axis, close to $\varepsilon_0=0^-$, namely, $E_0=1/\omega_0=\mathcal{O}(1/N)$. This is shown in the right panel of Fig. 14. Let us thus define $F'(z)=\bar{F}'(z)+1/(z-E_0)$, where $\bar{F}'(z)$ contains the roots on the arc. Taking only one root away from the arc does not modify the arc in leading order,[40] such that $\bar{F}_0'(z)=F_0(z)$. This means that in leading order, the roots on the arc are decoupled from E_0.

Let us now focus on the ground state of the central spin model with $h_0=\mathcal{O}(1)$. If we assume that the roots $E_{k=1,\ldots,M_b}$ in the ground state of the central spin model are still described by an arc in the complex plane for large particle number, we have $\gamma_1=-\bar{F}'(0)+\frac{1}{2d}+\frac{A_0}{2}-h_0$. This implies for the leading order $\gamma_1^{(0)}$

$$\gamma_1^{(0)}=-F_0(0)+\frac{1}{2d}+\frac{A_0}{2}-h_0 \tag{105}$$

$$=-\sum_{j=1}^{N_b}\frac{\sqrt{1+\delta^2A_j^2}}{2\sqrt{(\nu-A_j)^2+(A_j\delta)^2}}+\frac{1}{2d}-h_0, \tag{106}$$

where we have used the correspondence between BCS and central spin parameters in Eqs. (11) and (47). Note that $A_0=1/\varepsilon_0$ drops out in the first line.

The two parameters δ,μ are now determined by the asymptotes of $F_0(z)$

$$h_0=-\lim_{z\to\infty}F_0(z)=\frac{1}{2}\sum_{j=1}^{N_b}\frac{\nu A_j}{\sqrt{(\nu-A_j)^2+(A_j\delta)^2}}-\frac{\nu}{2\sqrt{1+\delta^2}}, \tag{107}$$

$$2S^z_{\mathrm{tot}} = -\lim_{z\to\infty} z[F_0(z)+h_0]$$
$$= \frac{1}{\sqrt{1+\delta^2}} + \sum_{j=1}^{N_b} \frac{\nu - A_j}{\sqrt{(\nu-A_j)^2+(A_j\delta)^2}}, \qquad (108)$$

where we have set $\varepsilon_0 = 0^-$. The first of these equations coincides with Eq. (41). The second Eq. (108) is identical to Eq. (40).

We have verified numerically that $\gamma_1^{(0)}+h_0=\mathcal{O}(1/N_b)$ for fields $h_0=\mathcal{O}(1)$. More generally, for $S^z_{\mathrm{tot}}=\mathcal{O}(1)$, the quantity $\gamma_1^{(0)}+h_0$ is of the order $\mathcal{O}(h_0^2/N_b)$ as can be seen from a simple physical argument: since the central spin is coupled to N_b bath spins, for $S^z_{\mathrm{tot}}=\mathcal{O}(1)$ it experiences an effective field h_0/N_b and so does each bath spin. Thus the leading h_0-dependent part of the spin-spin correlation function scales as $\sim h_0^2/N_b^2$, which yields a contribution $\sim h_0^2/N_b$ to the energy. For $S^z_{\mathrm{tot}}=\mathcal{O}(1)$ this is just the leading contribution from $\gamma_1^{(0)}+h_0$. For a small central field, this has been demonstrated in Eqs. (80), (82), and (88).

Since γ_1 is small compared to $\omega_0=\mathcal{O}(N_b)$, we can still use Eq. (69) to determine ω_0 iteratively. Thus Eq. (78) is still applicable for the energy, resulting now in

$$E_0 = -\frac{1}{4d} + \frac{h_0}{2} + \frac{\gamma_1^{(0)}}{2} - \frac{y_1^{(0)}}{2} - \frac{d}{2}[y_1^{(1)} - [y_1^{(0)}]^2 + y_2^{(0)} + h_0 y_1^{(0)}] + \mathcal{O}(d^2), \qquad (109)$$

$$= -\sum_{j=1}^{N_b} \frac{\sqrt{1+\delta^2 A_j^2}}{4\sqrt{(\nu-A_j)^2+(A_j\delta)^2}} - \frac{y_1^{(0)}}{2} - \frac{d}{2}[y_1^{(1)} - [y_1^{(0)}]^2 + y_2^{(0)} + h_0 y_1^{(0)}]. \qquad (110)$$

In the small-field limit, the results of the previous section are recovered.

Comparing Eq. (110) with Eq. (42), one identifies the leading classical contribution due to h_0 from Eq. (42) stemming from the roots on the arc, i.e., $\gamma_1^{(0)}$. The root ω_0 encodes additional quantum-mechanical fluctuations which are of the same order of magnitude as the classical h_0 terms.

In analogy to the energy, quantum fluctuations are also present in the correlation functions. In leading order, $\langle S_j^z\rangle$ is given by the classical expressions (38) and (39). Fluctuations are due to ω_0, which would yield a contribution $\sim d^2$ to $\langle S_j^z\rangle$, as in Eq. (67). However, the situation is different for the two-point function $\langle \boldsymbol{S}_0\cdot\boldsymbol{S}_j\rangle$: the quantum fluctuations in the energy lead to contributions of order $\mathcal{O}(d)$ in the two-point function, cf. Eq. (64). Taking together Eqs. (43) and (64), one obtains

$$\langle \boldsymbol{S}_0\cdot\boldsymbol{S}_j\rangle_0 = -\frac{(1+\delta^2)A_j - \nu}{4\sqrt{1+\delta^2}\sqrt{(\nu-A_j)^2+A_j^2\delta^2}} + \frac{d}{2}y_1^{(0)} - dA_j. \qquad (111)$$

Whereas Eq. (94) is valid in the weak-field regime $h_0<d$ only, Eq. (111) gives the field dependence and the leading finite-size effects also for stronger fields $h_0>d$. This result is compared to numerical data from complete diagonalization in Fig. 5, showing very good agreement. Moreover, from Eq. (111), it is clear how to separate classical from quantum fluctuations, giving nice insight into the essential physics of the model.

V. CONCLUSION

We have studied the exact solution of the central spin model, focussing on spectral properties and static correlators. In particular, it is possible to analyze the magnetization profile and the two-point correlation function using a classical approximation, exact diagonalization, and the Bethe-Ansatz solution as three independent methods.

The exact magnetization profile of the quantum model follows the classical approximation very well already for small system sizes. For a given distribution of coupling parameters an increasing central field typically enhances the antiparallel alignment between the central spin and the more strongly coupled bath spins nearby, while it favors parallel alignment with the bath spins further away. The total magnetization of the system is typically small.

For the two-point correlation function a similar tendency can be observed but the classical solution must be significantly corrected by quantum fluctuation terms as given in Eq. (111). Only for the outermost spins the classical solution tends to become exact. The reason for this is that in all cases we considered, classical contributions are encoded by the moments $x_{-\ell}$ of the couplings whereas quantum fluctuations are expressed in terms of the moments x_ℓ, $\ell>0$. This means that the outer region of the quantum dot, where the nuclear spins are coupled weakly to the electron spin, are governed by classical physics, whereas the inner region experiences stronger quantum fluctuations, due to the larger spin exchange.

The classical approach is analogous to the original BCS mean-field solution of the superconducting state. Typically the classical approximation works better for the BCS-model since quantum, i.e., finite-size contributions are subleading compared to the mean-field solution whereas in the central spin model both can be of the same order, depending on the quantity under consideration. The reason for this is that the pairing amplitude $g=\mathcal{O}(1/N)$ in the BCS model whereas the analogous parameter $h_0\equiv g^{-1}=\mathcal{O}(1)$ in the central spin model. In view of tunable interactions in ultracold gases, this could lead to the possibility of a new pairing phase for attractive electrons with fixed particle number, when the attraction g is of order 1.

After having demonstrated how to obtain the classical contributions from the exact quantum-mechanical solution, we must emphasize that if $h_0\neq 0$, the expectation value $\langle\Lambda|S_j^{x,y}|\Lambda\rangle$ vanishes for all eigenstates Λ. This is necessarily so since Λ must have a definite magnetization S^z_{tot} unless there is an accidental degeneracy in the system. For the equivalent BCS model this means that the BCS order parameter $\langle c^\dagger_{j\downarrow}c^\dagger_{j\uparrow}\rangle$ is identically zero for finite quantum systems. *Technically, the well-known spontaneous symmetry breaking can therefore only be realized in the thermodynamic limit in the BCS model, despite the fact that a description in terms of the mean-field solution (i.e., classical vectors* $\boldsymbol{m}_j$*)* also gives quantitatively good results for finite systems. This is in contrast to the prototypical example for symmetry breaking in ferromagnets, where the ground state and excited states generically already carry a nonzero expectation value of the order parameter for finite system sizes.

Our results are of direct importance for the study of nonequilibrium dynamics: the understanding of the magnetization profile of eigenstates allows us to estimate overlaps of eigenstates with those noneigenstates which are realistic initial states in the time evolution of the electron coupled to the nuclear spins. The computation of those overlaps is crucial in order to estimate the decoherence time. We leave this as a promising route for future research here. More generally, the study of classical and quantum contributions during the time evolution of nonequilibrium dynamics remains an important open question for future research.

ACKNOWLEDGMENTS

We are grateful to J.-S. Caux, F. H. L. Essler, M. A. Jivulescu, A. Klümper, Z. Kurucz, F. Göhmann, I. Schneider, and A. Struck for useful discussions. M.B. thanks the Rudolf-Peierls-Centre for Theoretical Physics, University of Oxford, for kind hospitality, where part of this work has been carried out. Financial support by the European network INSTANS and the SFB-TR49 is gratefully acknowledged.

*bortz@physik.uni-kl.de

[1] A. C. Johnson, J. R. Petta, J. M. Taylor, A. Yacoby, M. D. Lukin, C. M. Markus, M. P. Hanson, and A. C. Gossard, Nature (London) **435**, 925 (2005).
[2] A. V. Khaetskii and Y. V. Nazarov, Phys. Rev. B **61**, 12639 (2000).
[3] A. V. Khaetskii and Y. V. Nazarov, Phys. Rev. B **64**, 125316 (2001).
[4] J. Schliemann, A. V. Khaetskii, and D. Loss, J. Phys. Condens. Matter **15**, R1809 (2003).
[5] D. Loss and D. P. DiVincenzo, Phys. Rev. A **57**, 120 (1998).
[6] A. V. Khaetskii, D. Loss, and L. Glazman, Phys. Rev. Lett. **88**, 186802 (2002).
[7] A. Khaetskii, D. Loss, and L. Glazman, Phys. Rev. B **67**, 195329 (2003).
[8] J. Schliemann, A. V. Khaetskii, and D. Loss, Phys. Rev. B **66**, 245303 (2002).
[9] V. V. Dobrovitski and H. A. De Raedt, Phys. Rev. E **67**, 056702 (2003).
[10] W. A. Coish and D. Loss, Phys. Rev. B **70**, 195340 (2004).
[11] S. I. Erlingsson and Y. V. Nazarov, Phys. Rev. B **70**, 205327 (2004).
[12] Y. G. Semenov and K. W. Kim, Phys. Rev. B **67**, 073301 (2003).
[13] C. Deng and X. Hu, Phys. Rev. B **73**, 241303(R) (2006).
[14] K. A. Al-Hassanieh, V. V. Dobrovitski, E. Dagotto, and B. N. Harmon, Phys. Rev. Lett. **97**, 037204 (2006).
[15] W. A. Coish, E. A. Yuzbashyan, B. L. Altshuler, and D. Loss, J. Appl. Phys. **101**, 081715 (2007).
[16] W. Zhang, V. V. Dobrovitski, K. A. Al-Hassanieh, E. Dagotto, and B. N. Harmon, Phys. Rev. B **74**, 205313 (2006).
[17] G. Chen, D. L. Bergman, and L. Balents, Phys. Rev. B **76**, 045312 (2007).
[18] Z. Kurucz, M. W. Sorensen, J. M. Taylor, M. D. Lukin, and M. Fleischhauer, Phys. Rev. Lett. **103**, 010502 (2009).
[19] I. A. Merkulov, G. Alvarez, D. R. Yakovlev, and T. C. Schulthess, arXiv:0907.2661 (unpublished).
[20] R. Hanson, L. P. Kouwenhoven, J. R. Petta, S. Tarucha, and L. M. K. Vandersypen, Rev. Mod. Phys. **79**, 1217 (2007).
[21] W. A. Coish and J. Baugh, Phys. Status Solidi B **246**, 2203 (2009).
[22] M. Gaudin, J. Phys. (France) **37**, 1087 (1976).
[23] M. Gaudin, *La Fonction D'onde de Bethe* (Masson, Paris, 1983).
[24] E. K. Sklyanin, J. Sov. Math. **47**, 2473 (1989).
[25] J. von Delft and R. Poghossian, Phys. Rev. B **66**, 134502 (2002).
[26] M. Bortz and J. Stolze, Phys. Rev. B **76**, 014304 (2007).
[27] M. Gaudin, *Travaux de Michel Gaudin, Modèles Exactement Résolus* (Les Editions de Physique, CEA Saclay, 1995), p. 247.
[28] E. K. Sklyanin, Lett. Math. Phys. **47**, 275 (1999).
[29] P. Güttinger, Z. Phys. **73**, 169 (1932).
[30] W. Pauli, *Handbuch der Physik* (Springer, Berlin, 1933), p. 162.
[31] H. Hellmann, *Einführung in die Quantenchemie* (Franz Deuticke, Leipzig, 1937), p. 285.
[32] R. P. Feynman, Phys. Rev. **56**, 340 (1939).
[33] P. W. Anderson, Phys. Rev. **112**, 1900 (1958).
[34] M. C. Cambiaggio, A. M. F. Rivas, and M. Saraceno, Nucl. Phys. B **624**, 157 (1997).
[35] R. W. Richardson, Phys. Lett. **3**, 277 (1963).
[36] R. W. Richardson, Phys. Lett. **5**, 82 (1963).
[37] R. W. Richardson and N. Sherman, Nucl. Phys. **52**, 221 (1964).
[38] R. W. Richardson and N. Sherman, Nucl. Phys. **52**, 253 (1964).
[39] R. W. Richardson, J. Math. Phys. **6**, 1034 (1965).
[40] R. W. Richardson, J. Math. Phys. **18**, 1802 (1977).
[41] J. von Delft and D. C. Ralph, Phys. Rep. **345**, 61 (2001).
[42] J. Bardeen, L. N. Cooper, and J. R. Schrieffer, Phys. Rev. **108**, 1175 (1957).
[43] J. M. Román, G. Sierra, and J. Dukelsky, Nucl. Phys. B **634**, 483 (2002).
[44] E. A. Yuzbashyan, B. L. Altshuler, V. B. Kuznetsov, and V. Z. Enolskii, J. Phys. A **38**, 7831 (2005).
[45] S. Eggert, O. F. Syljuasen, F. Anfuso, and M. Andres, Phys. Rev. Lett. **99**, 097204 (2007).
[46] M. Takahashi, *Thermodynamics of One-Dimensional Solvable Problems* (Cambridge University Press, Cambridge, 1999).
[47] R. Hagemans and J.-S. Caux, J. Phys. A **40**, 14605 (2007).
[48] J. Richter and A. Voigt, J. Phys. A **27**, 1139 (1994).
[49] J. Richter, A. Voigt, S. E. Krüger, and C. Gros, J. Phys. A **29**, 825 (1996).
[50] E. A. Yuzbashyan, A. A. Baytin, and B. L. Altshuler, Phys. Rev. B **68**, 214509 (2003).
[51] S. Rombouts, D. Van Neck, and J. Dukelsky, Phys. Rev. C **69**, 061303(R) (2004).
[52] F. Dominguez, C. Esebbag, and J. Dukelsky, J. Phys. A **39**, 11349 (2006).